



RESEARCH ARTICLE

10.1029/2022JD036460

Key Points:

- An interdecadal trend (2000–2019) in an expansion of the Asian Summer Monsoon Anticyclone (ASMA) is found
- Expansion of the ASMA facilitates surface-to-upper troposphere and lower stratosphere transport of carbonaceous aerosols over the Asian monsoon regions
- Results are consistent with a rise of the tropopause due to the hydrostatic thermal expansion of the troposphere in a warming climate

Correspondence to:

W. K. M. Lau,
wkmiau@umd.edu

Citation:

Lau, W. K. M., & Kim, K.-M. (2022). Recent trends in transport of surface carbonaceous aerosols to the upper-troposphere-lower-stratosphere linked to expansion of the Asian Summer Monsoon Anticyclone. *Journal of Geophysical Research: Atmospheres*, 127, e2022JD036460. <https://doi.org/10.1029/2022JD036460>

Received 6 JAN 2022

Accepted 9 NOV 2022

Author Contributions:

Conceptualization: William K. M. Lau
Formal analysis: Kyu-Myong Kim
Funding acquisition: William K. M. Lau
Methodology: William K. M. Lau, Kyu-Myong Kim
Resources: Kyu-Myong Kim
Supervision: William K. M. Lau
Writing – original draft: William K. M. Lau
Writing – review & editing: William K. M. Lau, Kyu-Myong Kim

© 2022 The Authors.

This is an open access article under the terms of the [Creative Commons Attribution-NonCommercial License](#), which permits use, distribution and reproduction in any medium, provided the original work is properly cited and is not used for commercial purposes.

Recent Trends in Transport of Surface Carbonaceous Aerosols to the Upper-Troposphere-Lower-Stratosphere Linked to Expansion of the Asian Summer Monsoon Anticyclone

William K. M. Lau¹  and Kyu-Myong Kim²

¹Earth System Science Interdisciplinary Center (ESSIC), University of Maryland, College Park, MD, USA, ²Climate and Radiation Laboratory, Earth Science Division, NASA/GSFC, Greenbelt, MD, USA

Abstract Using Modern-Era Retrospective analysis for Research and Applications Version-2 (MERRA-2) re-analyses, we have examined recent trends (2000–2019) in transport of surface carbonaceous aerosols (CAs), that is, organic carbon and black carbon, to the upper troposphere and lower stratosphere (UTLS) during the Asian summer monsoon (ASM). We find a significant increased concentration of UTLS CA, linked to a linear trend in an expansion of the Asian Summer Monsoon Anticyclone (ASMA). Over core monsoon latitudes (25°–35°N), the trends in UTLS CA are enabled by increased upward transport from surface sources via an intensified monsoon meridional circulation, with increased latent heating over the southern Tibetan Plateau and foothill regions, enhanced by feedback processes associated with radiative heating by UTLS CA. In the extra-tropics, increased UTLS CA stems primarily from an extended source of increased wildfire emissions over eastern Siberia and northern Asia, coincident with a large-scale anomalous anticyclone with enhanced surface warming and drying near (80°–120°E, 55°–70°N). Here, CAs are transported upward from the surface to the ULS, likely by increased pyro-convection associated with enhanced wildfires, and enter the tropical UTLS via increased equatorward transport on the eastern flanks of anomalous upper-level anticyclones, coupled to the expanded ASMA. Overall, the increasing UTLS CA trends associated with expansion of the ASMA are consistent with a hydrostatic expansion of a warming troposphere, reflected in a rise in the tropical tropopause and consequential dynamical adjustments of the ASM subtropical jetstream, modulating the climate of the greater ASM region.

1. Introduction

Situated at approximately 10–20 km above sea level, the upper troposphere and lower stratosphere (UTLS) is a unique region in the earth's atmosphere that plays key roles in the radiative forcing and chemistry coupling of the earth's climate system. Found within the UTLS is the tropical (tropopause) transition layer (TTL) that separates the relatively well-mixed convective tropospheric air below from the radiatively controlled more stable stratosphere air above. The TTL exhibits chemical and dynamical properties of both the troposphere and the stratosphere, and is considered as the gateway for tropospheric air entering the stratosphere (Fueglistaler et al., 2009; Gettelman et al., 2002; Pan et al., 2014; Randel & Jensen, 2013). Substantial exchange of stratospheric and tropospheric air masses and chemical gases in the UTLS are known to occur across the TTL on time scales ranging from daily to interdecadal (Abalos et al., 2012; Frey et al., 2015; Manney et al., 2011; Müller et al., 2016; Pan et al., 2010; Phoenix et al., 2020; Ploeger et al., 2011, 2012; Randel & Jensen, 2013; Vogel et al., 2016). The air mass exchange strongly affects the distribution of water vapor, clouds, aerosol, ozone, and other chemical gases in the UTLS, which in turn can alter the amount of radiation absorbed by the atmosphere, and the surface thus modulating greenhouse warming effects (Dvortsov & Solomon, 2001; Kim et al., 2018; Riese et al., 2012; Solomon et al., 2011).

The Asian Summer Monsoon Anticyclone (ASMA), a dominant circulation feature of the Asian summer monsoon (ASM) in the UTLS has been identified as a major contributor to the transport of tropospheric and surface constituents to the UTLS and regions above (Basha et al., 2020; Clemens et al., 2022; Honomichl & Pan, 2020; Manney & Hegglin, 2018; Manney et al., 2021; Pan et al., 2016; Park et al., 2007, 2009; Preethi et al., 2017; Randel & Park, 2006; Randel et al., 2010; Santee et al., 2017; C. Shi et al., 2018). Numerous observational and modeling studies have revealed preferred pathways of transport of surface pollutants to the UTLS by tropical deep convection associated with the establishment of the ASMA, resulting in the formation of a distinctive

aerosol layer at approximately 13–18 km above sea level, within the TTL, that is, the Asian Tropopause Aerosol Layer (ATAL; Bossolasco et al., 2021; Fadnavis et al., 2013, 2017; Pan et al., 2016; Thomason & Vernier, 2013; Vernier et al., 2011, 2015; Yu et al., 2017). ATAL aerosols such as dust, black carbon (BC), and organic carbon (OC) are particularly important because of their capacity in absorbing solar radiation, thereby altering the atmospheric warming pattern, clouds, and water vapor distribution that in turn can provide regional aerosol-monsoon dynamical feedback (Fadnavis et al., 2017, 2019; Kim et al., 2015; Lau et al., 2016). Recently, Lau et al. (2018) identified the importance of intraseasonal deep convection over the southern and southeastern foothills of the Tibetan Plateau (TP) associated with internal variability of the ASMA in transporting surface pollutants over the mega-industrial complex of the Indo-Gangetic Plain (IGP) and the Sichuan Basin (SB) respectively to the UTLS. Upon entering the UTLS, the pollutants are advected around and confined within the ASMA, by the prevailing upper-level easterlies (westerlies) on the equatorward (poleward) portion of the ASMA, in the form of a Double Stem Chimney Cloud (DSCC), spanning East Asia to central Asia (120°–90°E, 20°–35°N), with the stem regions identified as the IGP and SB, respectively. Yuan et al. (2019) showed that there has been increasing loading of CA in the ATAL via the DSCC transport pathways, in conjunction with a strengthening of the ASM during 2000–2015. During the same period, Bossolasco et al. (2021) found positive trends in ATAL aerosols, including sulfate, primary and secondary organic aerosols, possibly linked to increased ice-nucleation in high clouds, associated with monsoon deep convection. In addition to transport from the surface and atmospheric boundary layer, ATAL constituents are found to be composed of mixture of air masses coming from different heights of the atmosphere, by way of diverse processes including entrainment by monsoon overshooting convection, anticyclone dynamics, stratospheric-tropospheric exchanges (STEX) due to eddy mixing associated with East Asian jetstream variability and Rossby wave breaking (RWB) events (Bian et al., 2020; Q. Fan et al., 2017; Lau et al., 2020; Riese et al., 2012; Samanta et al., 2016; Takemura et al., 2020). These processes are likely to be modulated in a warmer climate, and reflected in long-term changes in the ATAL constituents, and transport processes. At present, these changes and relationships with ASMA and jetstream variations remain poorly understood.

Because of the increasing threats of climate change on society, many recent studies have been focused on how surface pollutants, that is, greenhouse gases and aerosols from major anthropogenic emission sources are transported to the UTLS, and how they would interact with the earth climate system (Bian et al., 2020; Pan et al., 2016). However, under climate change, the earth system does not distinguish between natural versus anthropogenic aerosols, but rather interacts with total ambient (natural + anthropogenic) aerosols (Lau, 2016; Li et al., 2016). Globally, aerosols from natural sources are by far more abundant than from anthropogenic sources (d'Almeida et al., 1991; Satheesh & Moorthi, 2005). In particular, abundant emission and transport of natural aerosols such as wildfires, desert dust and sea salt in the greater ASM regions are likely to be affected by temperature, moisture, and winds changes under global warming. Hence, for better understanding effects of aerosol on ASM climate change, it is important to include, not only change in anthropogenic surface emissions, but also change in emissions and transport of natural aerosols that could also contribute to feedback processes spurred on by radiative forcing from anthropogenic emissions (Christian et al., 2019; Fadnavis et al., 2013; Lau et al., 2006; Li et al., 2016). Transport of surface pollutants to ATAL and STEEX are well known to be strongly affected by variability of the ASMA, and jetstream at UTLS levels in the subtropics and extratropics over a wide range of time scales from intraseasonal to inter-decadal (Bian et al., 2020; Gayatry et al., 2020; Pan et al., 2016; Park et al., 2007; Raga et al., 2022; Yuan et al., 2019). In this study, we focus on identifying basic mechanisms in the long-term trends in transport of CA from natural and anthropogenic sources to the UTLS over the greater ASM region. Specifically, we explore preferred pathways for transport of surface CA to UTLS, enabled by changes in precipitation, clouds, water vapor and diabatic heating, as well as possible aerosol-monsoon feedback processes, associated with a recent interdecadal trend in the expansion of the ASMA.

The organization of the rest of the paper is as follows. In Section 2, the approach and data used will be presented. In Section 3, we discuss the spatial distribution of the climatology and interdecadal trends in the ASMA and UTLS CA, and contemporaneous changes in the Asian monsoon climate states. This is followed by regression analyses in Section 4, linking the ASMA trend signals to preferred transport pathways of surface CA pollutant sources in the tropics and extratropics, in conjunction with changes in the East Asian subtropical jet, monsoon deep convection, and anticyclone dynamics. Trends in large-scale extratropical-tropical STEEX of CA, and linkage to changes in monsoon winds, precipitation, clouds, and possible feedback mechanism, modulating deep convection in the South Asian and East ASM will also be explored. In Section 4, relationship of the ASMA expansion and UTLS trends in CA to changes in tropopause height, in association with background warming of the greater

ASM ocean-land system during the data period will be examined. Summary and conclusions, as well as caveats of our results and need for further work to reduce uncertainties, are presented in Section 5.

2. Data and Methods

For our study, we use data from the NASA Modern-Era Retrospective analysis for Research and Applications Version-2 (MERRA-2) for the period 2000–2019, which include assimilation of aerosol optical depth (AOD) from the MODerate resolution Imaging Spectro-radiometer (MODIS) and Multi-angle Imaging Spectro-Radiometer (MISR) satellite observations during the Earth Observing System (EOS) era, 2000–present (Gelaro & Coauthors et al., 2017). MERRA-2 provides 4-dimensional high-resolution (3 hourly, 0.5° – 0.625° latitude-longitude, 72 vertical levels) global data of select chemical gases (ozone, CO, N_2O and others), aerosol species (sulfate, BC, OC, dust and sea salt) and meteorology from surface to the stratospheric, under all-weather conditions. To ensure consistency with independent observations, MERRA-2 rainfall products have been compared with data from Global Precipitation Climatology Project (GPCP), and aerosol products with Cloud Aerosol Lidar Pathfinder Satellite Observations (CALIPSO). Precipitation bias is corrected based on merged satellite-gauge data to provide better surface moisture fluxes, giving a more realistic MERRA-2 precipitation rate over land (Reichle et al., 2017). For aerosols, the satellite AOD are bias-corrected based on available data from the Aerosol Robotic Network (AERONET) ground-based observations (Buchard et al., 2017; Randles et al., 2017).

It is important to note that MERRA-2 aerosol data are not observations, but rather outputs of the NASA Goddard Earth System Model Version 5 (GEOS5) climate model constrained by state-of-the-art assimilations of both meteorological and AOD satellite observations. In cases where AOD observations are lacking, the re-analyses default to quantities generated by model physics. Daily emissions of BC and OC from biomass burning are derived from the Quick Fire Emission data set (QFED, Darmenov & da Silva, 2015) starting from 2010 to present, merged with bias-corrected earlier version of Global Fire Emission data (Duncan et al., 2003; Randerson et al., 2017; van der Werf et al., 2017). Anthropogenic emission of aerosols and precursory gases are derived from EDGARv4.2 (Diehl et al., 2012; European Commission, 2011; Janssens-Maenhout et al., 2019) up to the mid-2000's, depending on the availability of inventory for various gaseous species. For more recent periods (~mid-2000 to 2019), due to the unavailability of quality-controlled emission data suitable for data assimilation, emission inventory for the last available year was used repeatedly (Randles et al., 2017). For BC and OC, emission and surface concentration are constrained to be consistent with assimilated column AOD from MODIS and MISR, for the period of this study (2000–2019). In addition, MERRA-2 provides BC and OC subdivided into hydrophobic and hydrophilic species to account for their different rates of wet deposition, and interaction with atmospheric water. Because of the lack of recent updates in anthropogenic surface emission inventory in MERRA-2 as noted above, our study is mainly focused on better understanding of surface-to-UTLS transport of carbonaceous aerosols (CAs) linked to the expansion of the ASMA and possible feedback to the changing ASM climate. Relative importance of contributions from changes in surface emission versus transport in contributing to the UTLS aerosol loading cannot be addressed in this study. For linkage to climate warming signal in the tropics, we conduct trend analyses of ASMA expansion and associated changes in ASM circulation features with tropopause height, based on the cold-point-temperature (CPT) available from MERRA-2. It is well recognized that CPT is an appropriate measure of tropopause height for the tropics, but has large uncertainties for the extratropics due to transient wave perturbation (Gettelman et al., 2009; Munchak & Pan, 2014; Pan et al., 2018). For completeness, we have included CPT tropopause analyses including the extratropics. Hence, our results on trend signals in tropopause height in the extratropics have to be taken with extreme caution, and need to be assessed with other definitions of tropopause height, and intercomparison of multiple reanalyses in further studies (Tegtmeier et al., 2020; Wilcox et al., 2012). For statistical significance, we use the Student's two-tail test.

3. Results

Climatologically during June–July–August, the ASMA is the dominant feature of the UTLS over the eastern hemisphere (Figure 1a), characterized by a planetary scale anticyclone spanning eastern Africa to the western Pacific, with elevated geopotential height (GPH), strong easterlies in the tropics (5° – 25° N), westerlies in the extratropics (30° – 45° N), and strong equatorward (poleward) meridional flow on the eastern (western) flank of the ASMA (e.g., Dunkerton, 1995; Ge et al., 2018; Hsu et al., 1999; Krishnamurti et al., 1973; B. Liu et al., 2013;

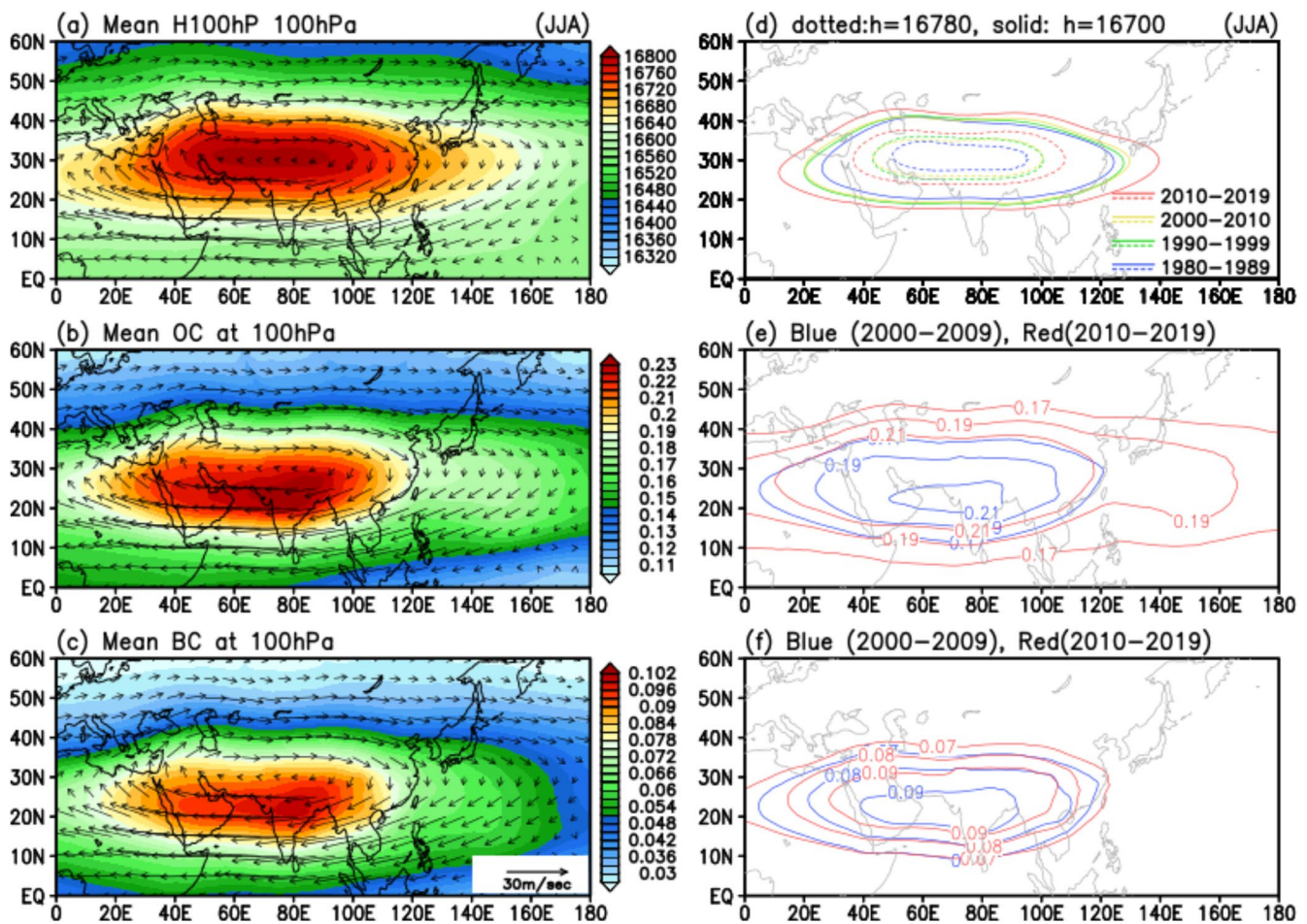


Figure 1. Climatology of (a) Asian Summer Monsoon Anticyclone (ASMA), represented by 100 hPa geopotential height (m), (b) OC and (c) black carbon (BC) mixing ratio ($\mu\text{g}/\text{kg}$). Representative contours showing decadal mean areal extent of (d) ASMA represented by iso-heights of 16,780 m (dotted) and 16,700 m (solid), (e) organic carbon (OC) mixing ratios at 0.17, 0.19, and 0.21 $\mu\text{g}/\text{kg}$ and (f) BC mixing ratios at 0.07, 0.08, and 0.09 $\mu\text{g}/\text{kg}$, during different decades from 1980 to 2019.

Manney et al., 2021). The ASMA has strong control on the climatological distribution of CA in the UTLS, with the maximum loading mostly confined within the ASMA (Figures 1b and 1c).

As can be seen in the contours of representative GPH height levels (Figure 1d), the areal extent of the ASMA as defined here has substantially expanded from the previous (1980–1999) to the more recent decades (2000–2019). Similarly, representative contours indicating high concentrations of OC and BC (Figures 1e and 1f) show substantial areal expansion during the last two decades. The area expansion of OC appears to be more extensive compared to BC, with the representative contours extending over the western Pacific. This is likely due to the stronger presence of more diffusive fine particulate organic matters contributing to the OC loading (Randles et al., 2017; Soto-Garcia et al., 2011). The time series of areal extent of representative GPH contours, CA concentration (Figure 2a), and respective areal mean values (Figure 2b) show strong linear trends during the last four decades. The trend in areal expansion of the ASMA in MERRA-2 is consistent with previous studies on long-term trends on areal extent, shape, and higher moments of the ASMA, based on multiple re-analyses data, for overlapping periods (Basha et al., 2020; Manney & Hegglin, 2018; Manney et al., 2021; Santee et al., 2017). Worth noting here is that MERRA-2 AOD assimilation is based on NOAA AVHRR data over oceans from 1980 to 2000, but switched to NASA MODIS and MISR covering both ocean and land, from 2000 to present. As a result, linear trend analyses involving aerosols across the two periods (before and after 2000) is likely to encounter larger uncertainties, and possibly systematic bias due to different qualities of the assimilated satellite products (Buchard et al., 2017; Randles et al., 2017). Accordingly, results presented in this study are based only on the latter 20 yr period, that is, 2000–2019, where only NASA satellite products are assimilated in MERRA-2. A 20 yr period is

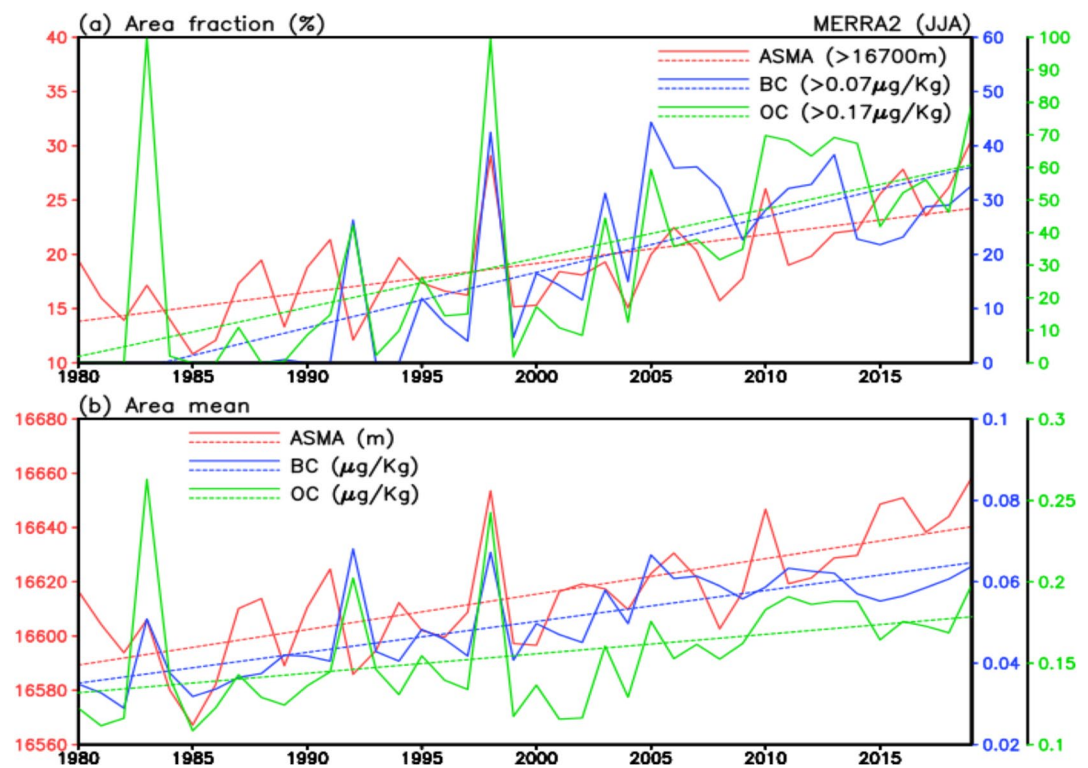


Figure 2. Time series of (a) area fraction (%) exceeding a representative level shown in Figure 1 for Asian Summer Monsoon Anticyclone (ASMA) geopotential (>1,6700 m, red), organic carbon (OC) (>0.17 μg/kg, green) and black carbon (BC) (>0.07 μg/kg, blue) relative to the total area shown in Figure 1, and (b) areal mean values of geopotential height(m, red), OC(μg/kg, green) and BC(μg/kg, blue) within the selected areas used in panel (a).

obviously too short to isolate global warming trends. The term “linear trend” used in this study is likely to reflect also interdecadal variability of the UTLS circulation, including the well-known Silk Road Pattern over Eurasian during boreal summer (Han et al., 2021; Hong & Lu, 2016; Y. Liu et al., 2020; N. Shi et al., 2019; Stephan et al., 2019; L. Wang et al., 2017).

3.1. UTLS CA Trend Patterns

Given the highly non-uniform distributions of CA sources, winds, and precipitation over the greater ASM regions to be addressed in our analyses, the transport of aerosol from surface sources to the UTLS is highly 3-D in nature. To emphasize the UTLS signals, we first show the climatology and trend patterns for CA loadings above 500 hPa, in 2-D latitude-height (Figure 3), and longitude-height (Figure 4) cross-sections respectively. Climatologically, during June–July–August (JJA), the latitude-height sections of OC and BC (Figures 3a and 3b) over the ASM region (70°–130°E) show enhanced UTLS loading over two distinct regions, that is, the core Asian summer monsoon region (ASMR, 20°–35°N) and the extratropical regions (EXTR, 50°–80°N), separated by a rapid drop of the tropopause height across the tropopause break (TBR, 35°–45°N, 250–150 hPa) with ill-defined tropopause height, and where isentropic exchange of air masses and constituents between the tropical UT and extratropical LS occurs frequently during the boreal summer (Bian et al., 2020; Boothe & Homeyer, 2017; Holton et al., 1995; Yang et al., 2016, and many others). For OC (Figure 3a), the primary climatological contribution appears to come from EXTR, with a secondary contribution from ASMR. In contrast, relatively higher loading of BC is found over ASMR than EXTR (Figure 3b). These features in climatological distributions of UTLS CA are consistent with increased anthropogenic emissions of BC from industrialization and economic growth in ASMR, and increased emission of OC from frequent outbreak of severe wildfires in boreal forests of East Siberia/Northeast Asia in recent decades (Groisman et al., 2007; Kharuk et al., 2021; Mokhov & Chernokulsky et al., 2010; Yasunari et al., 2021).

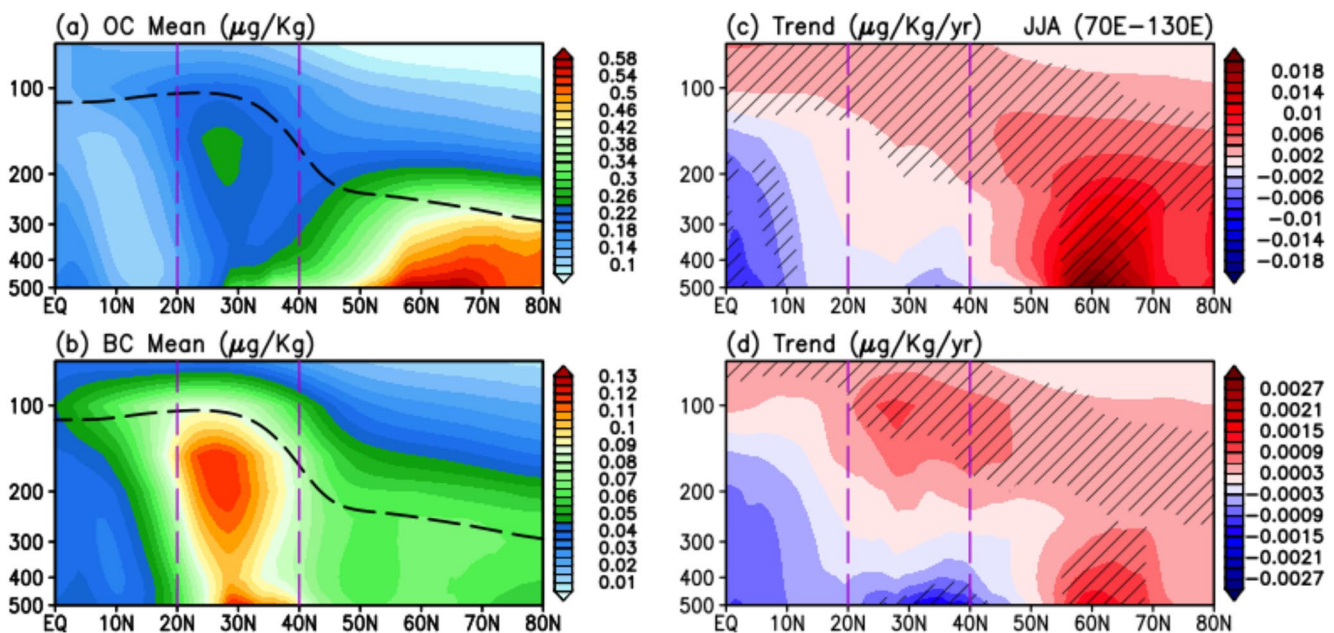


Figure 3. Latitude-height climatological profiles averaged over 70–130°E for (a) organic carbon (OC), and (b) black carbon (BC). Thick black dashed lines indicate climatological tropopause height. Panels (c and d) are the same as (a and b) respectively, except for linear trend pattern during 2000–2019. Purple vertical dashed lines indicate latitude bounds of the climatological Asian Summer Monsoon Anticyclone (ASMA). Regions exceeding 95% significance are indicated by slashes.

The linear trend of OC (Figure 3c) reveals an apparent source over the EXTR, reflecting increased upward and equatorward transport into the tropical LS (near and above 100 hPa) coupled to a strong apparent sink over the deep tropics and the ASMR. The trend pattern for BC (Figure 3d) suggests similar apparent sources, sinks, and transport pathways as in OC, except that the apparent source over EXTR is weaker than the sink over the ASMR near 400–500 hPa, compared to OC.

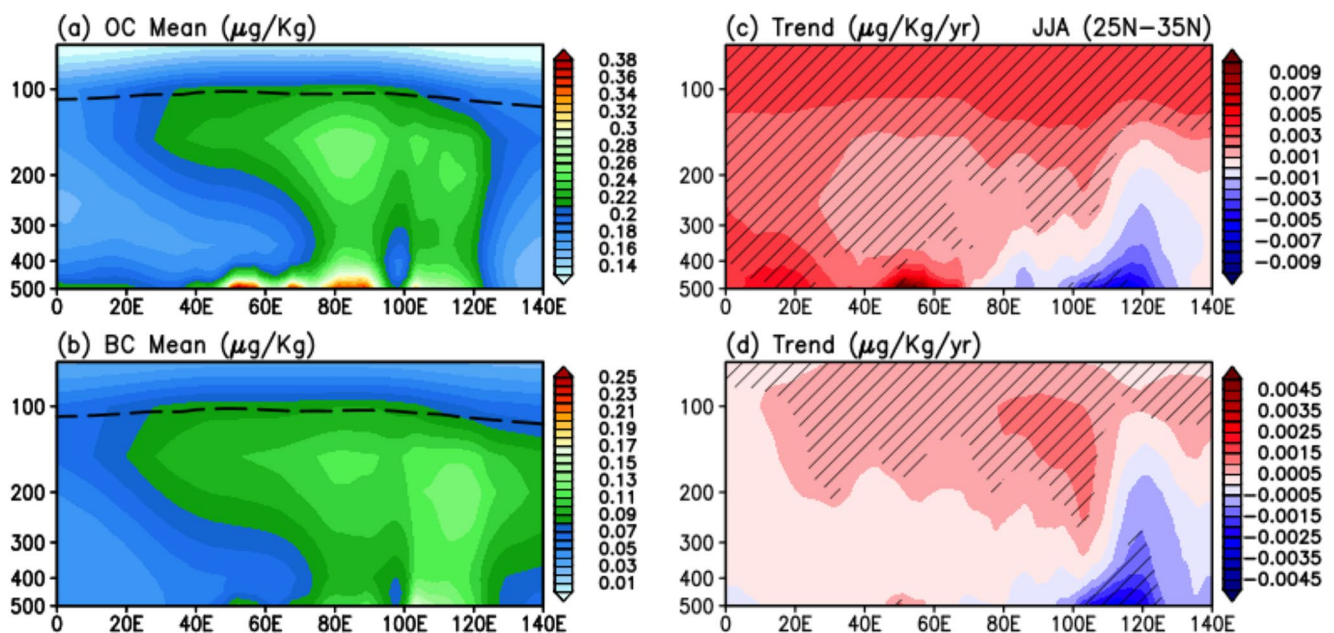


Figure 4. Longitude-height climatological profiles averaged over the core Asian monsoon region (25°–35°N) for (a) organic carbon (OC) and (b) black carbon (BC). Dashed black lines indicate climatological tropopause height. Panels (c and d) are the same as (a and b) respectively, except for linear trend pattern during 2000–2019. Regions exceeding 95% significance are indicated by slashes.

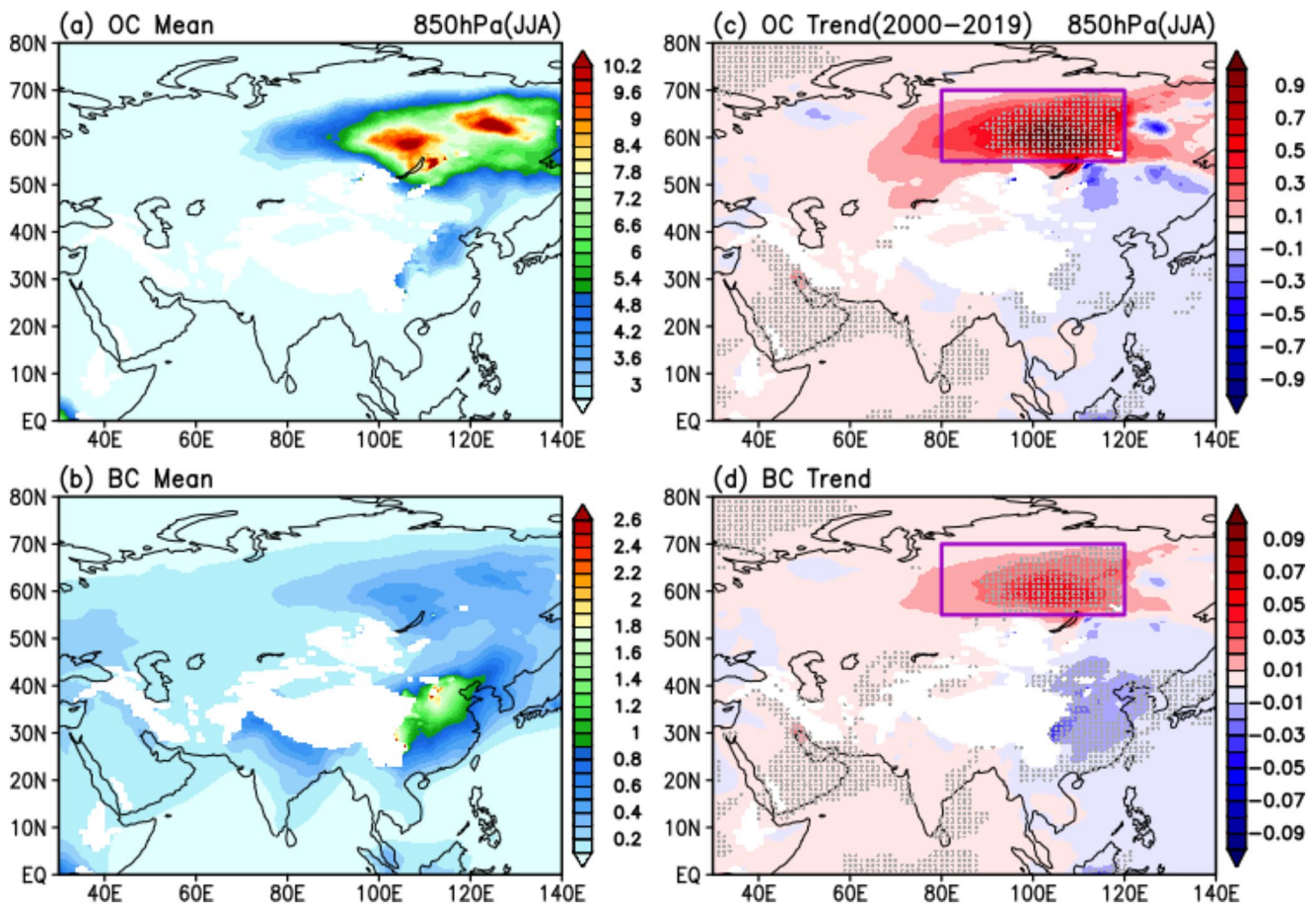


Figure 5. Climatological spatial distribution of (a) organic carbon (OC) and (b) black carbon (BC) at 850 hPa. Units are in $\mu\text{g}/\text{kg}$. Panels (c and d) are the same as for (a and b) except for linear trend pattern during 2000–2019 ($\mu\text{g}/\text{kg yr}^{-1}$). The area with large increasing trend in the extratropics (55° – 70°N , 80° – 120°E) is indicated by a rectangle. Regions exceeding 95% significance are indicated by gray dots.

Over the ASMR, the longitude-height cross-sections of the meridional means (25° – 35°N) of climatological UTLS OC and BC (Figures 4a and 4b) show respectively the DSCC pattern that has been linked to surface emission sources over the industrial mega-cities complex of the IGP in northern India (70° – 90°E), and the Sichuan Basin (100° – 110°E) in southwestern China respectively (Lau et al., 2018; Yuan et al., 2019). Positive trends in UTLS OC and BC (Figures 4c and 4d) respectively are found across the entire longitude span (30° – 140°E), except over the Asian monsoon regions (80° – 130°E), where a negative trend for OC and BC in the mid-to- upper troposphere (UT; 500–200 hPa) is found, reflecting increased precipitation washout (See Section 3.2 for further discussion). The increased OC and BC in the LS over the ASMR is consistent with the equatorward transport noted previously (Figures 3c and 3d). The positive trends in OC and BC, particularly the former, in the LS (near and above 100 hPa), appear to be more uniformly distributed in the east-west direction, suggesting the greater importance of large-scale horizontal transport and diffusive mixing in OC compared to BC. The relationships among the UTLS CA 2-D trend patterns (Figures 3 and 4) and the 3-D changes in climatic states of the ASM linked to the trend in the expansion of the ASMA (Figures 1 and 2) will be explored in the rest of the paper.

3.2. Transport of Surface Pollutants to UTLS

Here, we first examine the climatological distributions of near-surface OC and BC from MERRA-2. While different in regional details, the JJA near-surface (850 hPa) climatologies of OC and BC loadings (Figures 5a and 5b) show overall similar distributions indicating common, but spatially inhomogeneous, emission sources over north-eastern Asia that extend westward across EXTR and ASMR, except over high mountain terrains. These emission sources are consistent with observations from satellite and in situ measurements indicating strong contributions of

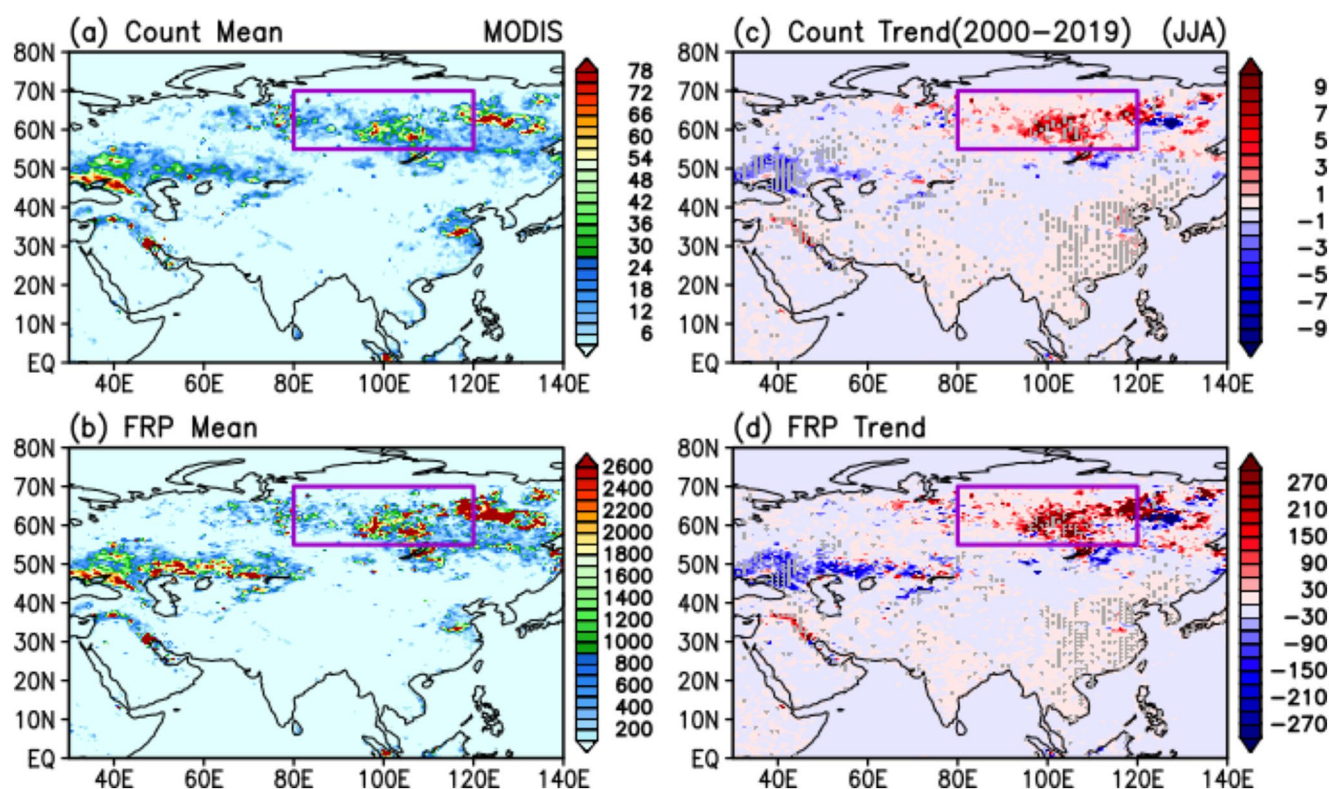


Figure 6. Climatological distribution of June–July–August seasonal total (a) fire pixel count (days) and (b) fire radiative power (W/m^2) from MODIS onboard Terra satellite. Panels (c) and (d) are the same as for (a) and (b) except for linear trend pattern during 2000–2019. The area with large increasing trend in the extratropics ($55^\circ\text{--}70^\circ\text{N}$, $80^\circ\text{--}120^\circ\text{E}$), is indicated by a rectangle. Regions exceeding 95% significance are indicated by gray dots.

CA from frequent large-scale wildfires in boreal forests of Siberia and northeastern Asia (Groisman et al., 2007; Yasunari et al., 2018), as well as from industrial pollutions in the ASMR (Bian et al., 2020; Lau et al., 2018; Pan et al., 2016; Yuan et al., 2019; and many others).

The linear trend pattern depicts a prominent increase in near-surface loading of OC and BC (Figures 5c and 5d) spanning northern Eurasia ($55^\circ\text{--}70^\circ\text{N}$, $80^\circ\text{--}120^\circ\text{E}$). The climatology and positive trend in CA in the EXTR are consistent with the spatial patterns of MODIS fire count (Figures 6a and 6c), and Fire Radiative Power (Figures 6b and 6d) during the same data period, as well as extended drought conditions with increased wildfires over northeastern Eurasia reported in previous studies for a data period overlapping with ours (Groisman et al., 2007; Meng et al., 2015; Yasunari et al., 2018; Zhang et al., 2019). For BC (Figure 5d) a negative trend is found over the East Asian monsoon region ($20^\circ\text{--}50^\circ\text{N}$, $110^\circ\text{--}120^\circ\text{E}$). The negative trend in BC over East Asia is likely due to increased wash-out by enhanced precipitation (see discussion for Figure 7). It may also reflect in part reduced emission due to clean air policies implemented by East Asian countries since the mid-2000's (S. X. Wang et al., 2014; Zeng et al., 2019; Zheng et al., 2018) that resulted in a decreased burden of near-surface CAs that is captured by the MERRA-2 AOD assimilation. The relationships among the near-surface CA concentration, UTLS transport and changes in climatic state of the ASM are examined next.

During 2000–2019, the ASM witnessed an inter-decadal trend featuring a northward displacement of the ASM rain belt (Figure 7a) with enhanced precipitation near $20^\circ\text{--}50^\circ\text{N}$, most pronounced over the Himalayan foothill regions of the Tibetan Plateau (TP), coupled to reduced precipitation in the deep tropics ($0^\circ\text{--}20^\circ\text{N}$) and in subpolar latitudes ($55^\circ\text{--}70^\circ\text{N}$). The precipitation displacement is associated with increased low-level southwesterlies over East Asia and the establishment of a low-level anomalous cyclonic circulation cell near ($110^\circ\text{--}130^\circ\text{E}$, $20^\circ\text{--}55^\circ\text{N}$), transporting moisture to and increasing near-surface relative humidity (RH) in northeastern Asia (Figure 7b). The cyclonic circulation appears to be coupled to a large-scale dry (reduced precipitation and RH) near-surface anticyclone, centered near $55^\circ\text{--}70^\circ\text{N}$, $80^\circ\text{--}120^\circ\text{E}$, co-located with the

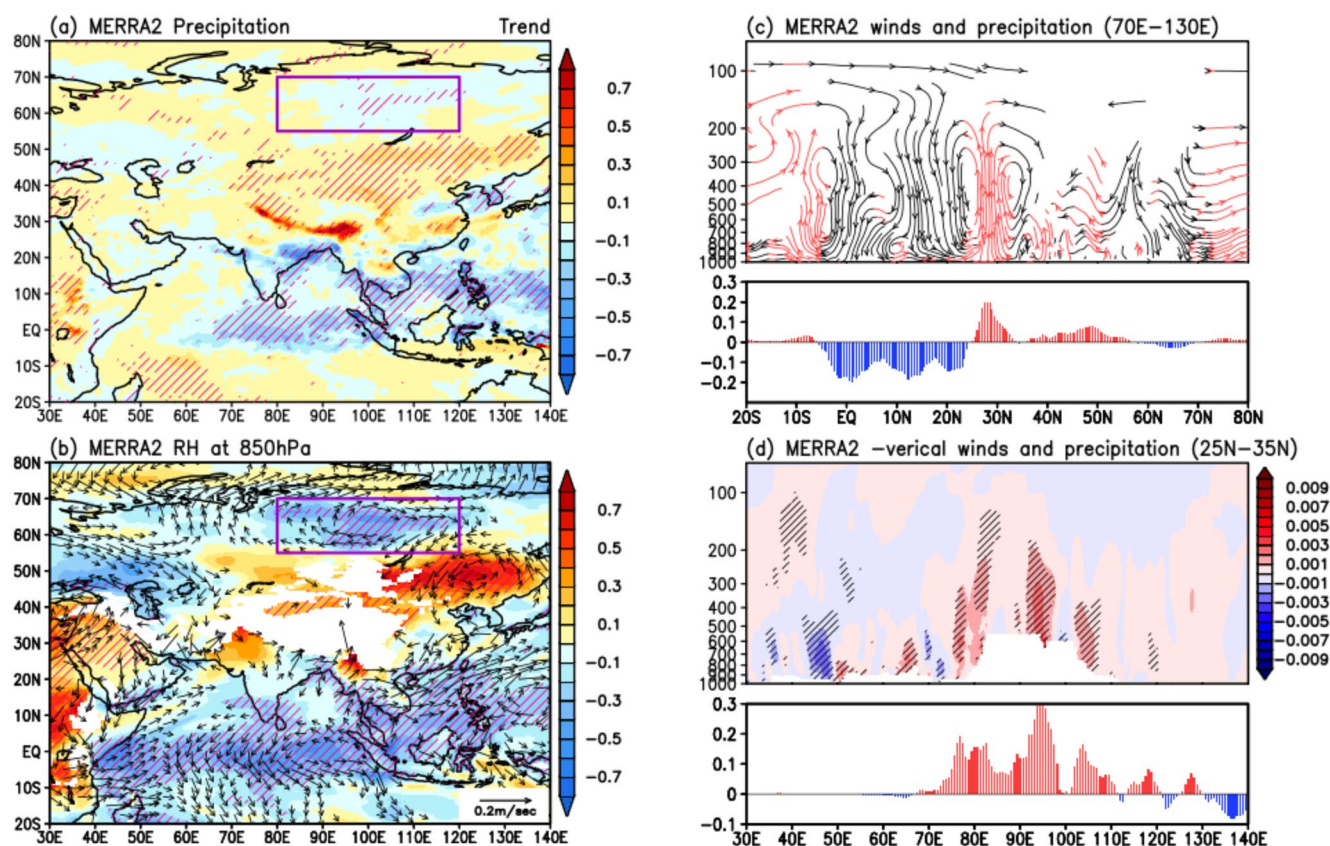


Figure 7. Linear trend pattern of (a) precipitation and (b) 850 hPa relative humidity and winds over the greater Asian monsoon regions. Right panels show (c) linear trend of latitude profiles of meridional monsoon circulation and precipitation averaged over 70°–130°E, with red streamline indicating rising motion and (d) longitude profiles of vertical motions and precipitation averaged over core Asian monsoon regions (25°–35°N). Rectangle boxes in (a) and (b) mark the region of maximum enhanced source of carbonaceous aerosols, as shown in Figures 5 and 6. Slashes indicate regions exceeding 95% significance.

enhanced near-surface CA sources (see Figures 5 and 6). It can also be identified as a component of an extratropical planetary-scale wavetrain pattern, identified by anomalous circulation cells spanning extratropical Eurasia (30°–140°E, 40°–70°N) in Figure 7b. The aforementioned trends in precipitation and RH are underscored by a long-term trend in a tightening of the Monsoon Meridional Circulation (MMC) with strong anomalous ascent and increased precipitation over the core ASMR (25°–35°N), coupled to broad scale descent and decreased precipitation in the deep tropics (0°–20°N), as well as anomalous sinking motions in the extratropics (50°–70°N, Figure 7c) coinciding with the location of surface anticyclone (Figure 7b). Across the extended east-west longitudes (30°–140°E) of the core ASMR, maximum increases in precipitation and ascending motions are found over TP and foothill regions (Figure 7d), signaling the importance of increased condensational heating as well as orographic uplifting in facilitating transporting surface pollutants to the UTLS (Lau et al., 2018; Park et al., 2009; Yuan et al., 2019).

Next, linear regression analyses using the least squares approach were conducted to examine the linkages of the ASMA expansion trend (Figure 2a) to surface-to-UTLS transport of CA, and to changes in the ASM climate states (Figure 7). UTLS OC (Figures 8a and 8c) and BC (Figures 8b and 8d) in the EXTR appear to originate from the climatological pollutant sources over the anomalous surface anticyclone near 55°–70°N (see Figure 7b), likely via increased ascent by enhanced pyro-convection associated with increased wildfires (Cunningham & Reeder, 2009; Trentmann et al., 2006). Subsequently, OC/BC in the extratropical LS are transported across the TBR (35°–45°N) to the tropical UTLS (Figures 8c and 8d) via increased equatorward meridional winds on the eastern side of anomalous anticyclones linked to the ASMA expansion (see discussion in Section 3.3). Over the ASMR, there is a strong reduction of OC and BC due to removal by increased wet deposition associated with enhanced precipitation over the region (Ji et al., 2015; Yan et al., 2019).

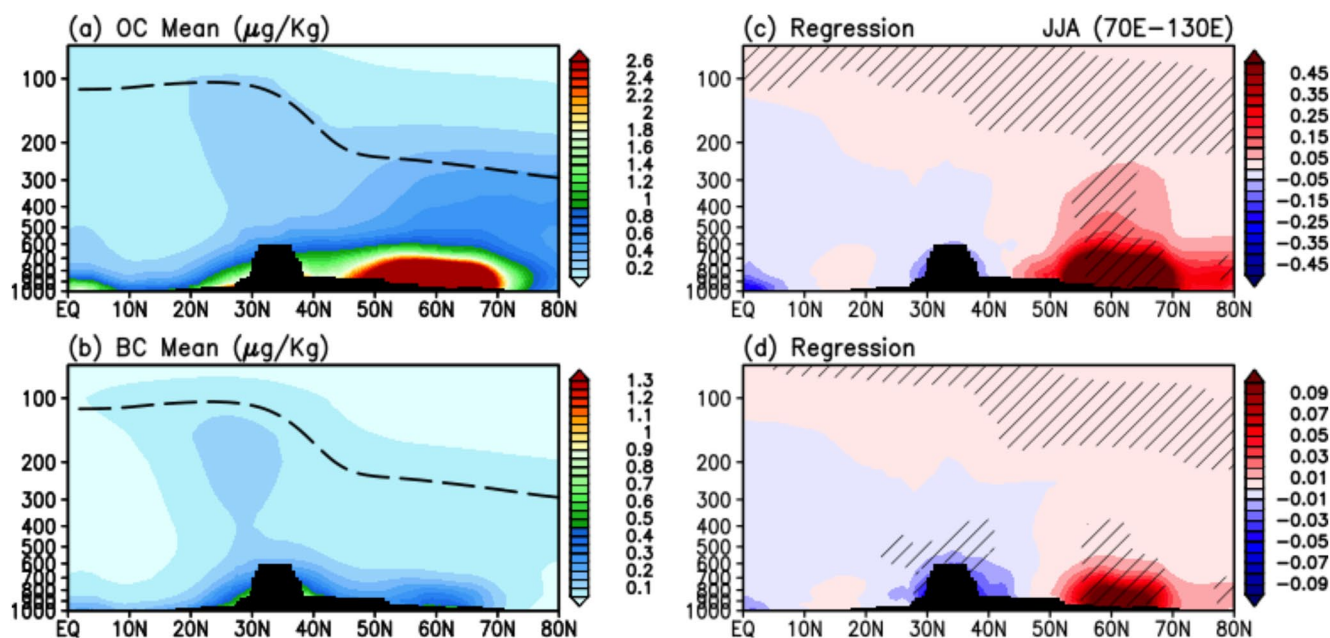


Figure 8. Climatology of surface-to-UTLS latitude-height profiles for (a) organic carbon (OC) and (b) black carbon (BC) averaged between 70°E and 130°E. Panels (c) and (d) are the same as (a) and (b) respectively, except for linear regressions with time series of Asian Summer Monsoon Anticyclone (ASMA) expansion during 2000–2019. Thick black dashed lines indicate climatological tropopause height. Regions exceeding 95% significance are indicated by slashes.

Along the core ASMR latitudes (25°–35°N), strong sinks for OC (Figures 9a and 9c) and BC (Figures 9b and 9d) are found over the climatological sources of eastern Himalayan foothills and East Asia, due in part to the removal by increased precipitation. Reduced emission from clean air policy in East Asia, reflected in the assimilated MODIS AOD, during the data period may also have contributed to the OC/BC reduction (see further discussion in Conclusion).

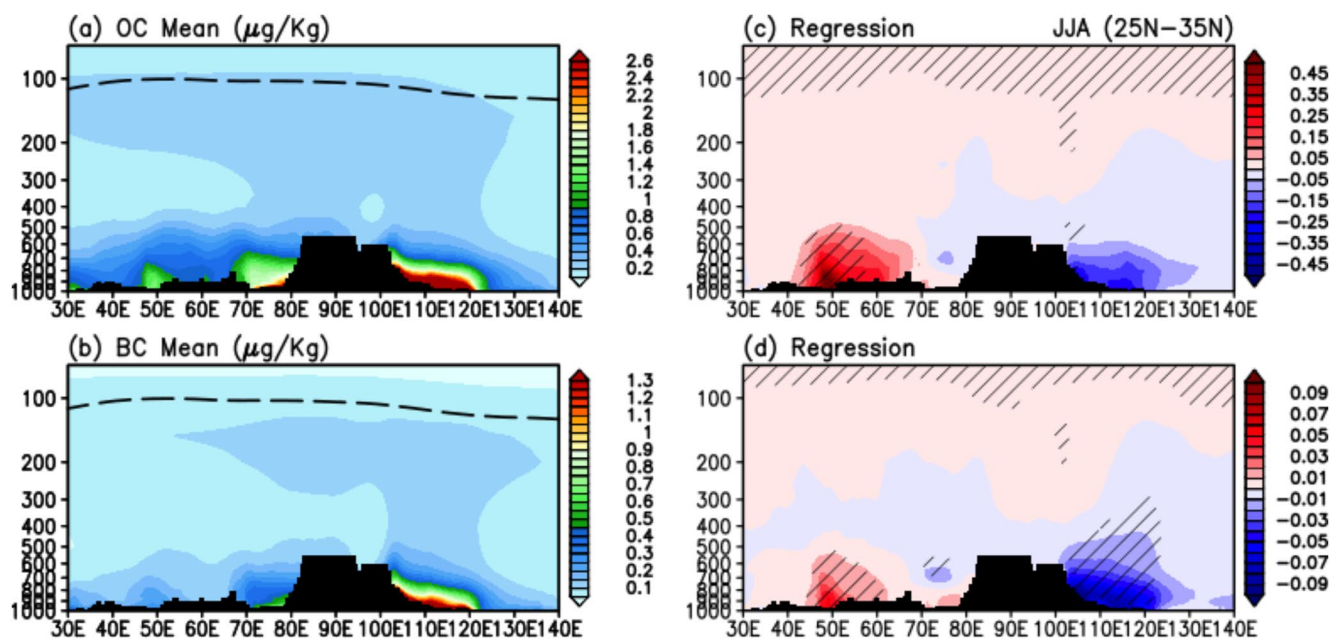


Figure 9. Climatology of surface-to-UTLS longitude-height profiles over core Asian monsoon region (25°–35°N) for (a) organic carbon (OC) and (b) black carbon (BC). Panels (c) and (d) are the same as (a) and (b) respectively, except for linear regression with time series of Asian Summer Monsoon Anticyclone (ASMA) expansion. Thick black dashed lines indicate climatological tropopause height. Regions exceeding 95% significance are indicated by slashes.

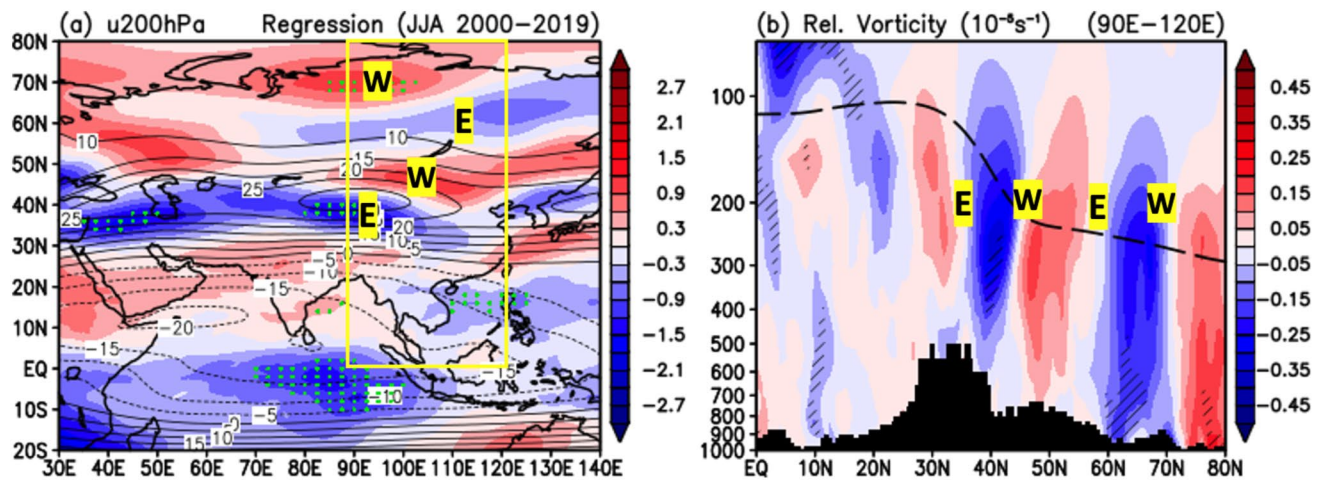


Figure 10. Linear regression coefficients with Asian Summer Monsoon Anticyclone (ASMA) expansion for (a) horizontal distribution of zonal winds (ms^{-1}) at 200 hPa, (b) latitude-height profiles of relative vorticity (10^{-5} s^{-1}) averaged between 90°E and 120°E . Contours in (a) indicate 200 hPa zonal wind climatology. Labels E (W) represents approximate locations of 200 hPa maximum anomalous easterlies (westerlies). The yellow rectangular box in (a) represents the domain where the latitude-height profile of relative vorticity in (b) has been computed. Thick black dashed lines in (b) indicate climatological tropopause height. Green dots in (a) and slashes in (b) indicate exceedance of 95% statistical significance.

3.3. UTLS Wavetrain and Transport Processes

Here, linkages of the ASMA expansion to transport of near-surface CA to the UTLS and possible feedback mechanisms affecting the ASM climate are further examined. Regression analyses for zonal winds and vorticity with respect to the ASMA expansion trend have been conducted. The zonal wind regression pattern (Figure 10a) shows a northward displacement of the subtropical jetstream, most pronounced in the jet entrance region (30° – 70°E), consistent with recent findings of positive correlation between jetstream latitude and ASMA centroid location, both shifting northward, with ASMA expansion in recent decades (Manney et al., 2021). Near the jet exit region (90° – 120°E), alternating anomalous easterlies and westerlies can be seen emanating from the ASMA climatological region (20° – 40°N) into the far northern extratropics, and regions further eastward over the western North Pacific. The meridional-height cross-section of anomalous relative vorticity (Figure 10b) shows alternating signs of barotropic vorticity anomalies extending from the UTLS region to the surface, consistent with effects of anticyclonic RWB associated with variability of the subtropical jet that accompanies the development of extreme hot/dry summer conditions in the northeast ASM regions (Enomoto et al., 2003; Homeyer & Bowman, 2013; Takemura & Mukougawa, 2020; Takemura et al., 2020). The near quadrature (90° out-of-phase) relationship of 200 hPa zonal winds and relative vorticity indicates the important role of changes in the meridional gradient of the 200 hPa winds associated with the poleward shift of the ASM jetstream in determining the preferred overturning locations of RWB.

The quadrature relationship between relative vorticity and zonal wind changes is consistent with the latitude-height profiles of zonal winds regressed onto the ASMA expansion trend (Figure 11a). Here, the pattern depicts a northward shift of 200 hPa westerlies near the exit region (90° – 120°E) of the East Asian subtropical jet and the concomitant development of an equivalent barotropic wavetrain with deep vertical structure that emanates from the TBR (35° – 45°N) into the subpolar near surface regions. The establishment of the deep surface-to-UTLS anomalous anticyclone in 55° – 70°N (regions marked by the letter “A” in Figure 11), with anomalous westerlies (easterlies) to the north (south) of the zero-wind line, coincides almost exactly with the CA surface sources due to increased wildfires in extratropical northern Asia (see Figure 5). Over the center of the anticyclones, transport of air mass and pollutants from the extratropical LS near 200 hPa into the tropical UTLS is increased by enhanced equatorward flow (negative meridional winds in Figure 11b) on the eastern side of the expanded ASMA. The anomalous zonal and meridional winds are accompanied by strong ascent (descent) over the Tibetan Plateau/Himalayan foothills (deep tropics, 0° – 20°N), coupled to alternate rising (sinking) motion over cyclonic (anticyclonic) centers in extratropical regions (Figure 11c). Over the entire domain, an increase in high cloud fraction in the LS, just above the climatological tropopause, is noteworthy (Figure 11d). In regions of enhanced vertical motion near 25° – 30°N , increased clouds are due to the development of deep convection transporting additional

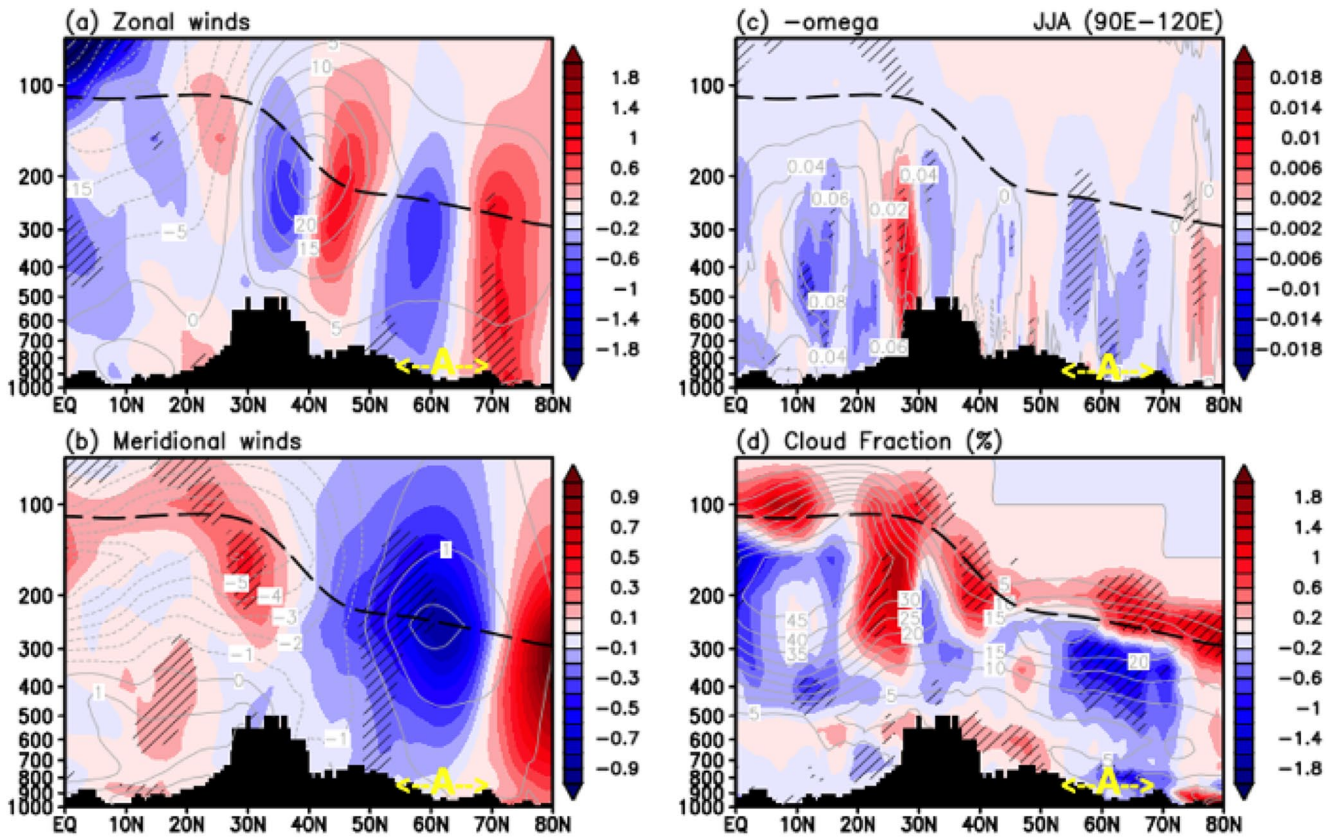


Figure 11. Latitude-height profile of regression coefficients with Asian Summer Monsoon Anticyclone (ASMA) expansion for (a) zonal winds (ms^{-1}), (b) meridional winds (ms^{-1}), (c) vertical motion (Pa s^{-1}), and (d) cloud fraction (%), over East Asian regions (90° – 120°E). Grey contours represent climatology of the respective fields. Yellow label A indicates the location (55° – 70°N) of the near-surface anomalous anticyclone and CA emission source identified previously (Figures 5–7). Thick black dashed lines indicate climatological tropopause height. Slashes indicate exceedance of 95% statistical significance.

moisture from below. In the deep tropics and in anticyclonic regions (marked by A in Figure 11) in the extratropics where anomalous subsidence and near-surface CA loadings dominate (See Figure 5), the increase in clouds in the LS appears to occur at the expense of clouds in the UT (Figure 11d). Changes in UTLS clouds resemble the trend pattern in relative humidity (Figure 12a). Calculations to identify the relative roles of temperature versus moisture in causing changes in clouds have been conducted based on the Clausius-Clapeyron (CC) relationship governing relative humidity (RH): $\delta\text{RH} = \delta q/q_s - \alpha \text{RH} \delta T$, with $\alpha = L(R_v T^2)^{-1} \sim 6.5\% \text{ K}^{-1}$, where L is the latent heat of condensation, and R_v , the ideal gas constant, q and q_s the ambient and saturated specific humidity respectively. Results indicate that the linearized CC-relationship (Figure 12b) is a reasonable approximation to the trend pattern in RH in MERRA-2 (Figure 12a). Increased clouds in UTLS are due mostly to increased upward transport of moisture over the Tibetan Plateau and foothill regions (Figure 12c). On the other hand, warming of the UT ($\delta T > 0$) increases the saturated specific humidity, leading to reduced RH and less clouds (Figure 12d). To provide context for these results, we note that cloud processes in MERRA-2 are parameterized by a prognostic scheme that includes evaporation, auto-conversion, accretion of cloud water and ice, sedimentation of cloud ice, and re-evaporation of falling precipitation, initiated by exceedance of empirical critical RH thresholds, constrained by assimilation of Atmospheric Infrared Sounder observations (Bacmeister et al., 2006; Molod, 2012; Molod et al., 2015). Hence, our results provide only a first order qualitative estimate of changes of RH-cloudiness relationship in the troposphere and the UTLS associated with the ASMA expansion, as simulated by the climate model underlying MERRA-2. For better understanding the effects of moisture and temperature changes on UTLS ice clouds, further analyses of homogeneous and heterogeneous nucleation processes based on RH over ice from observations and multiple reanalyses need to be conducted.

Over the latitude of the core ASMR region (25° – 35°N), the long-term trend in reduction in columnar total CA is contributed mainly by hydrophilic OC/BC (Figures 13a and 13c), which has high affinity for water, and is subject

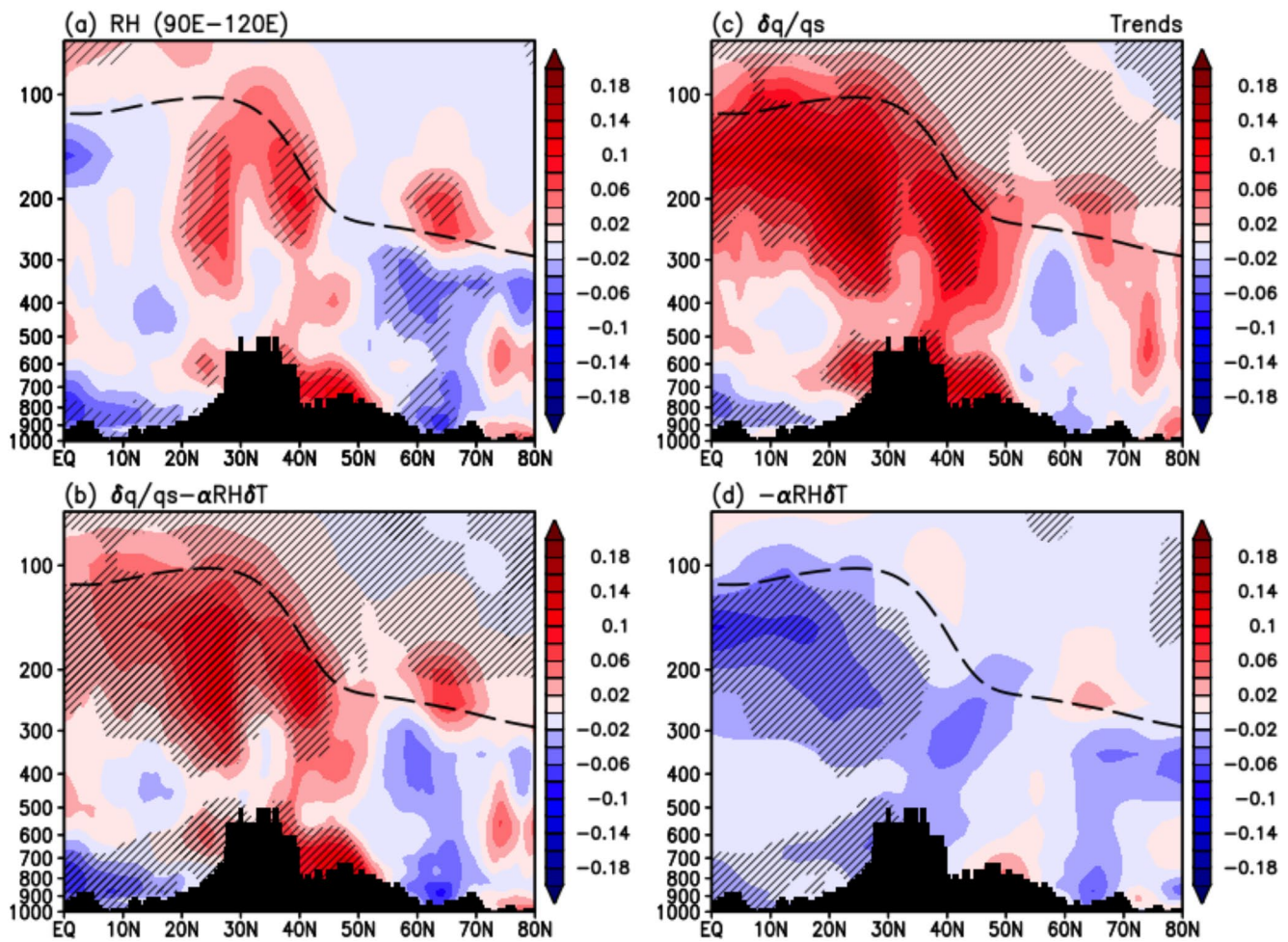


Figure 12. Latitude-height profile of linear trends over the Asian Summer Monsoon Anticyclone (ASMA) region (90°–120°E) for (a) relative humidity and (b) combined effects of moisture and temperature trends on relative humidity based on the linearized Clausius-Clapeyron equation for recent two decades (2000–2019). Panels (c and d) show moisture and temperature contribution, respectively. Units are in change (%) per year. Thick black dashed lines indicate climatological tropopause height. Slashes indicate exceedance of 95% statistical significance.

to rapid removal by dissolution and wet deposition. However, in spite of the reduction of total OC/BC, there is a significant increase in non-water soluble hydrophobic OC/BC in the UTLS over the Tibetan Plateau due to increased vertical transport of pre-existing ambient OC/BC in the mid-troposphere to the UTLS (Figures 13b and 13d). The UTLS hydrophobic OC/BC aerosols facilitate the increase in cloud fraction and cloud water (liquid and ice) in the UTLS (Figures 14a and 14b) by enhancing cloud condensation and ice nucleation processes (e.g., Fadnavis et al., 2013, 2017; J. Fan et al., 2016; Hendricks et al., 2011; Rosenfeld et al., 2014, 2008; Rosenfeld & Woodley, 2000). Heating due to absorption of solar radiation by elevated hydrophobic BC/OC and trapping of longwave radiation by increased UTLS clouds (Figure 14c) can enhance moisture convergence from below, providing a positive feedback to increased condensational heating over the Tibetan Plateau (Figure 14d). The long-term increases in cloud fraction, cloud water (liquid and ice), radiative and condensation heating in the UTLS are consistent with the Elevated Heat Pump (EHP) dynamical feedback induced by absorbing aerosols (OC/BC and dust) facilitating orographic forced ascent and enhanced diabatic heating over the Tibetan Plateau, enhancing the ASMA (Lau et al., 2006, 2008).

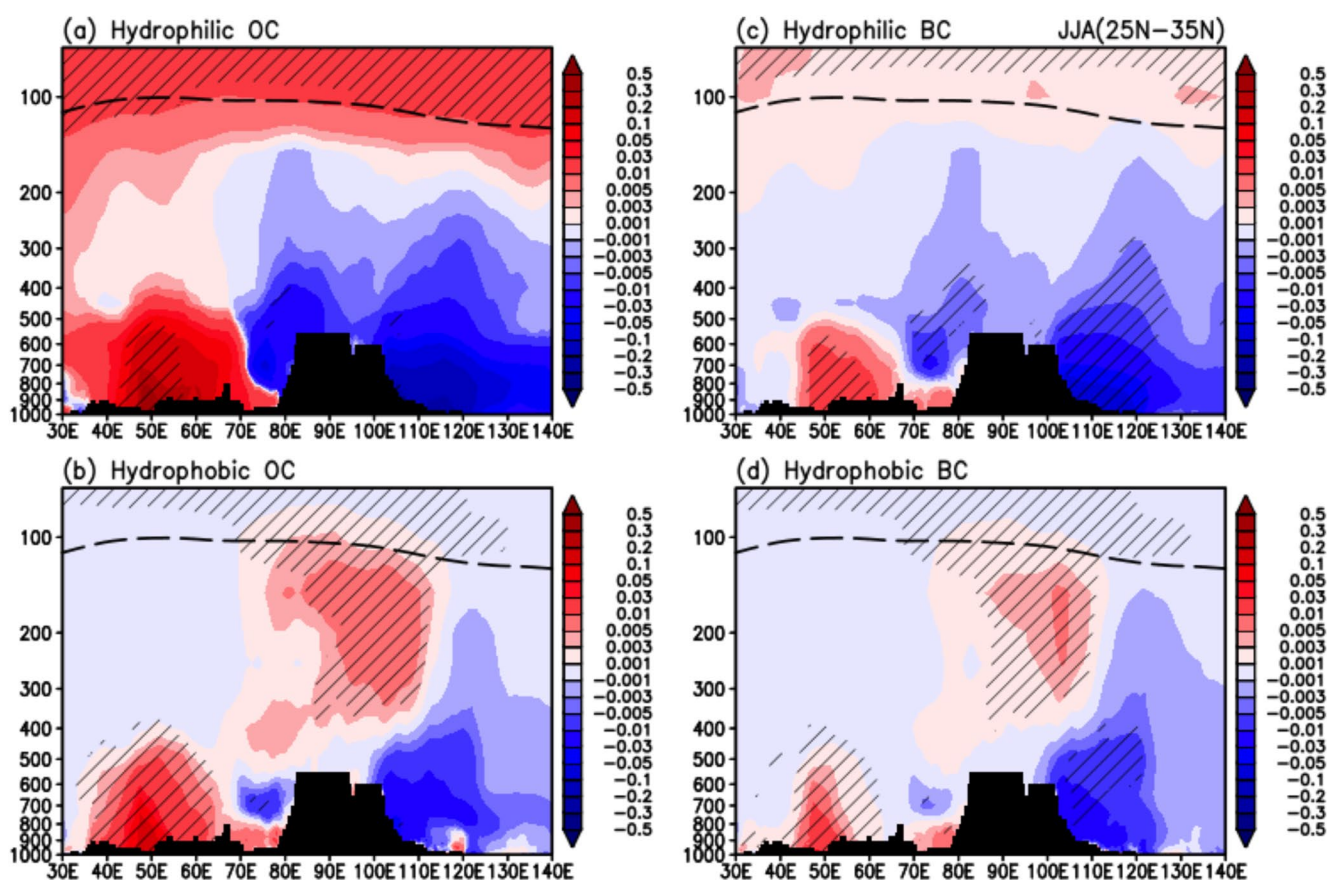


Figure 13. Longitude-height profiles of regression coefficient with Asian Summer Monsoon Anticyclone (ASMA) expansion for (a) hydrophilic organic carbon (OC), (b) hydrophobic OC, (c) hydrophilic black carbon (BC) and (d) hydrophobic BC, over the core Asian monsoon region (25°–35°N). Units are in $\mu\text{g}/\text{kg yr}^{-1}$. Thick black dashed lines indicate climatological tropopause height. Slashes indicate exceedance of 95% statistical significance.

4. ASMA Expansion and UTLS Transport in a Warming Climate

In this section, we examine the relationships among the ASMA expansion and UTLS transport in the context of a warming climate over the greater Asian monsoon region. Recent modeling and observational studies have identified key signals of global warming, in the form of a rise of the tropical tropopause, coupled to a widening descending branch of the Hadley Circulation, with increased drying of the subtropical-extratropical continent (Byrne & Schneider, 2016; Dai, 2013; Lau et al., 2013; Lau & Kim, 2015; Santer, Sausen, et al., 2003; Santer, Wehner, et al., 2003; Seidel et al., 2008; Seidel & Randel, 2006; Su et al., 2017; Trenberth et al., 2014; Voigt & Shaw, 2015). Recent studies have also indicated that regional shifts in the Hadley and Walker Circulations, arising from both natural variability and climate change could lead to non-uniform widening of the tropics as a function of longitudes and seasons (D'Agostino et al., 2020; Sohn et al., 2019; Staten et al., 2019; Yun et al., 2021). Here, we are focused on the linkages of ASMA expansion to the warming of the greater ASM regions, including Eurasia, the tropical western Pacific and India Ocean, during JJA for the 2000–2019 period. As shown in Figure 15a, during this period, the tropopause height as defined by the cold-point temperature (Munchak & Pan, 2014; Zhou et al., 2001) over the greater Euro-Asian monsoon influence region (0° – 80°N , 40° – 160°E) has been rising near uniformly in the tropics (0° – 20°N) at a rate of 0.2–0.3 hPa/yr. Over the northern flank and regions further north of the climatological ASMA (30° – 40°N), quasi-stationary wave-like perturbations characterized by an elevated (depressed) tropopause in regions with anticyclonic (cyclonic) circulations are found. Per discussion in Section 3, these tropopause-level circulation anomalies are strongly linked to the ASMA expansion and increased CA loading in the UTLS over the greater Asian monsoon region during the same period. Enhanced equatorward northerlies on the eastern flank of the major anomalous anticyclones (labelled A_1 , A_2 , A_3 in Figure 15a) provide conduits for equatorial transport of air mass and pollutants from the extratropical LS to tropical UTLS. Anticyclone A_1 and A_2 , and a cyclonic circulation in between are consistent with nonlinear effects of RWB, resulting

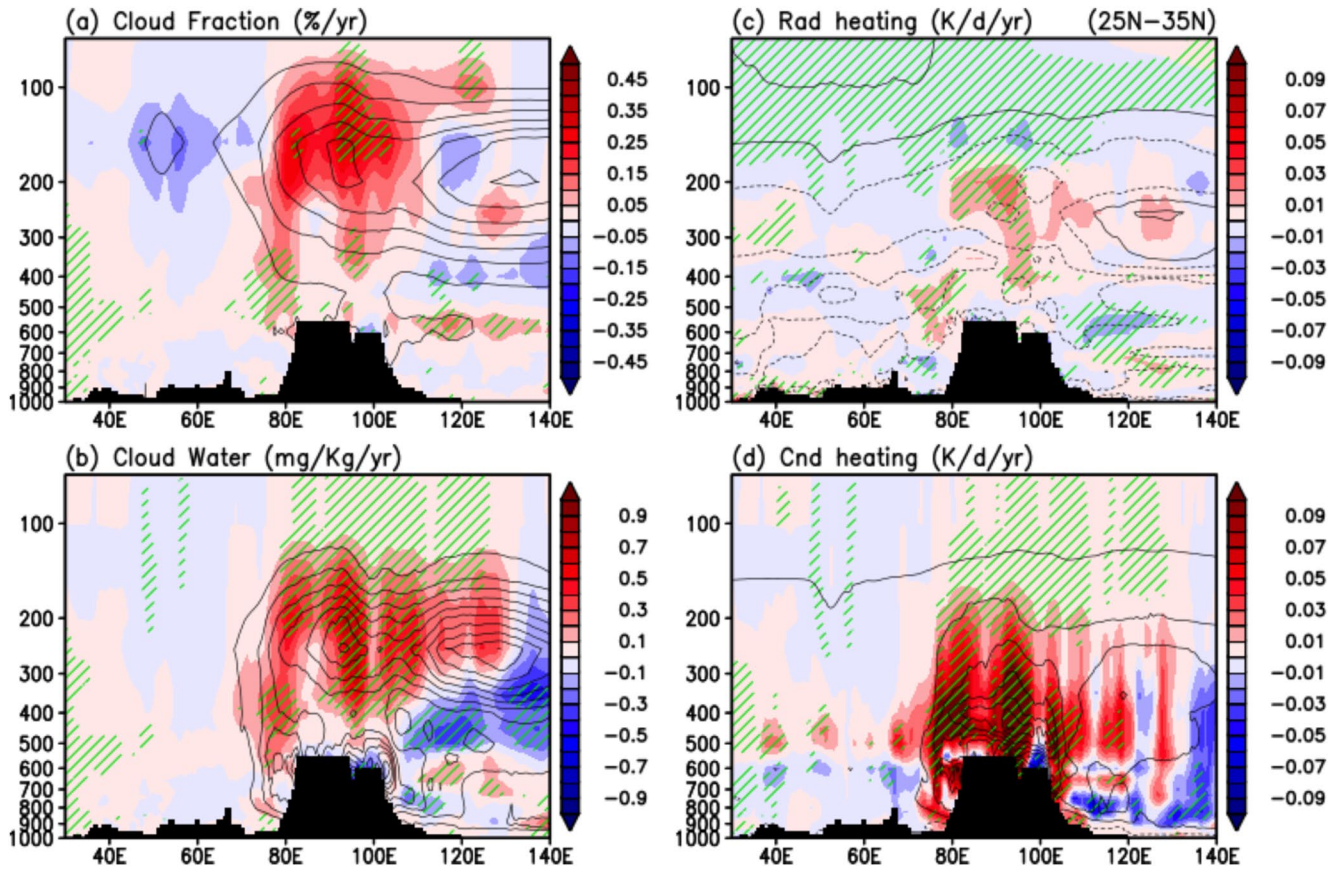


Figure 14. Linear trend pattern (2000–2019) of longitude-height profiles of (a) cloud fraction, (b) cloud water (liquid + ice), (c) radiative heating, and (c) condensation heating over core Asian monsoon region (25°–35°N). Climatological means are shown as contour, and regions exceeding 95% significance are shown as green slashes.

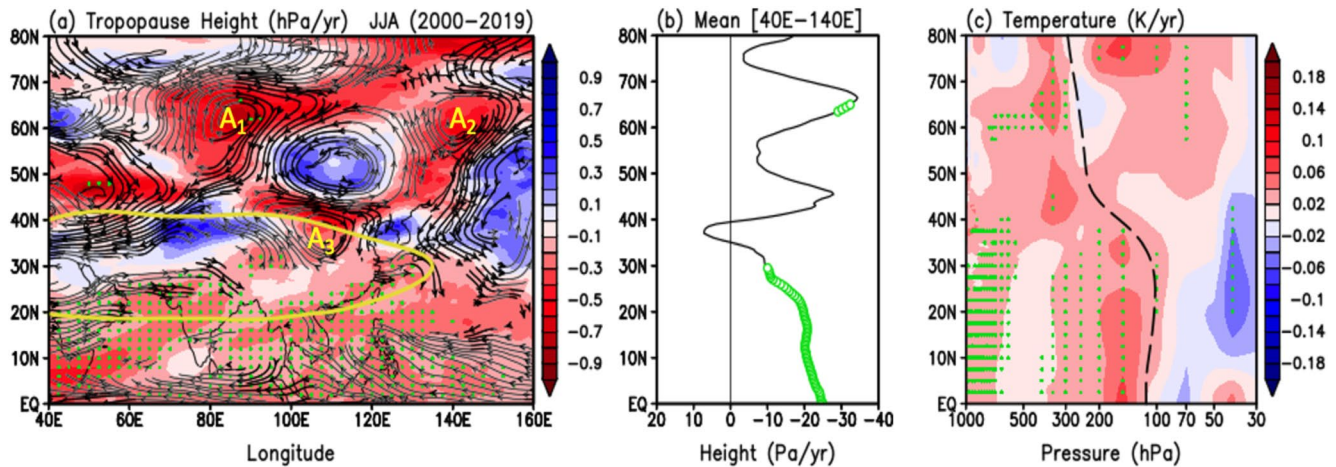


Figure 15. Linear trend pattern (2000–2019) for (a) tropopause height (hPa yr^{-1}) and streamflow at climatological tropopause level, with red (blue) shading indicating rising (sinking) tropopause, and equatorward flow highlighted in dark black color on the eastern side of major anomalous anticyclones (A1, A2, and A3). Yellow contour indicates climatological mean 100 hPa iso-height of 16,700 m, as a proxy of the mean location of Asian Summer Monsoon Anticyclone (ASMA); (b) latitude profile of zonal mean (40°–140°E) trend in tropopause height; (c) same as in (b), except for vertical profile of temperature trend from surface to 30 hPa over the same domain.

from ASMA expansion and increased anticyclonic shear due to the northward shift of the jetstream near the jet exit region (90° – 120° E) over East Asia (see Figure 10a). The anomalous anticyclone A_3 can be attributed to a Gill-type Rossby-wave response (Gill, 1980), forced by enhanced latent heating due to increased precipitation over the Tibetan Plateau and foothills regions of the ASMR core domain (see Figures 7a and 7d), and modified by jetstream shifts associated with the ASMA expansion (Figure 10a). Enhanced atmospheric CA stemming from increased wildfires and injected into the UTLS by pyro-convection in the EXTR during the peak monsoon season are transported to downstream regions over northern and northeast Asia by the prevailing upper-level westerlies, and subsequently enter the tropical UT by increased southward winds on the eastern flank of ASMA anticyclones. The anomalous southward winds in A_2 and A_3 are particularly effective in enhancing the equatorward flow on the eastern flank of the climatological ASMA (see Figure 1), resulting in increased UTLS loading of CA over East Asia and the western Pacific. In the zonal mean across 40° – 160° E (Figure 15b), the tropopause in the tropics is raised quasi-uniformly. Over the extratropics, the tropopause shows wave-like variations associated with RWB, featuring elevated heights most pronounced in anticyclonic regions, 40° – 50° N, and 60° – 70° N. The zonal mean vertical profile of the temperature trend (Figure 15c) depicts an overall warming of the troposphere over the entire region, with enhanced surface warming in the tropics, and warming in the UT in the regions of rising tropopause (Figure 15b) just below the TTL due to hydrostatic expansion of the troposphere (increase in volume due to warming of an atmospheric column under its own weight) and rise of warmer surface air following the moist adiabatic lapse rate. These processes lead to enhanced high clouds and increased moistening and warming of the UTLS (see Figures 11d and 12), resulting in changes of the UTLS radiative balance, with net gain in upwelling longwave radiation from below. As less upwelling radiation can reach higher levels in the tropical stratosphere, cooling by net loss in radiation tends to occur in the LS and regions above (Forster & Shine, 1999, 2002; Gettelman et al., 2010; Rosenlof & Reid, 2008). In the polar and subpolar stratospheric regions ($>70^{\circ}$ N), changes in ozone heating, modulated by inter-decadal planetary scale waves, could be another important factor affecting stratospheric temperature and moisture changes in the stratosphere (Hartmann et al., 2000; Shepherd, 2008). However, ozone heating and interaction with polar stratospheric planetary waves are subjects outside the scope of this investigation.

5. Conclusions

Using MERRA-2 data, we have investigated issues arising from the key science question of how an inter-decadal trend in the expansion of the ASMA could have affected the transport of surface carbonaceous pollutants to the UTLS during 2000–2019. Key findings of this study are summarized as follow:

1. ASMA in a changing ASM climate

- There is a robust trend in the expansion of areal extent of the ASMA, and increased loading of UTLS CA over the influence regions of the ASMA, during 2000–2019.
- Also found is a corresponding trend in the Asian monsoon climate, characterized by a tightening of the MMC, a northward shift of the East Asian jet near the exit region (90° – 120° E) with enhanced precipitation and convective ascent over 25° – 35° N coupled to increased drying (reduced precipitation and relative humidity) in extensive regions to the south (0° – 20° N) and in extratropical (50° – 70° N) land regions.
- The trend in ASMA expansion is likely associated with long-term (inter-decadal) effects in UTLS winds reflecting increased anticyclonic Rossby Wave Breaking (RWB) in the extratropics. Key features include a northward displacement of the East Asian subtropical jetstream, excitation of equivalent barotropic quasi-stationary waves and increased transport of CA from surface to UTLS affecting East Asia and downstream regions.

2. ASMA and UTLS transport

- The ASMA expansion trend is coupled to extensive drying in the extratropical land region in association with the development of a large-scale surface anticyclone over northern and northeastern Asia (55° – 70° N, 80° – 120° E), concomitant with enhanced CA emissions from increased wildfires and pyro-convection that facilitate ascent of CA to the lower stratosphere (LS). Upon entering the LS, CA is transported equatorward on the eastern flank of anticyclonic cells embedded in the expanded ASMA to the tropical UTLS over East Asia and the western Pacific.
- Over the core ASM region, increased precipitation washout leads to reduced total BC/OC loading in the troposphere, limiting entry of BC/OC into the UTLS. However, in spite of the reduction in total BC/OC,

hydrophobic BC/OC aerosols, which do not interact with water and are less affected by precipitation wash-out, are injected into UTLS by the increased large-scale ascent associated with the tightening of the MMC. Heating by absorption of solar radiation of these aerosols may have played an important role in intensifying the MMC via the EHP aerosol-monsoon feedback mechanism (Lau et al., 2006, 2008).

- Overall features of CA UTLS transport and ASMA expansion are consistent with a large-scale warming trend over the greater ASM region (0°–70°N, 40°–160°E), manifested in a rise of the tropical tropopause height associated with a hydrostatic thermal expansion of a warming troposphere, and increased moistening and cooling of the LS, consistent with the effect of greenhouse warming.

It is important to note that MERRA-2 re-analyses for CA in our study are not observations, but rather adjusted model outputs that are dynamically consistent with assimilated satellite observations. The paucity of reliable satellite observations of aerosols due to orbital constraints, contamination from clouds and bright earth surface over desert, and snow and ice cover are major limiting factors for the MERRA-2 re-analyses. In the absence of satellite assimilation constraints, aerosol distributions default to model physics. MERRA-2 has a proven record in producing high-quality meteorology and aerosol products for weather and climate studies. However, for multi-decadal trend studies that require consistent satellite and ground observation inputs over long periods, large uncertainties may arise. Specifically, for anthropogenic emission of CA, MERRA-2 used the EDGAR V4.2 industrial emission inventory only up to 2005–2007, after which the final year of emission is persisted up to the present (Randles et al., 2017). Hence, effects of recent clean air acts implemented by East Asian countries on anthropogenic CA emission inventory have not been included in MERRA-2 emission inventory. However, because of the assimilation of MODIS and MISR AOD throughout our data period (2000–2019), the decreasing trend in atmospheric loading of BC and OC over the ASMR in MERRA-2 attributed to increased precipitation wash-out in this study, may also be caused in part by reduction in anthropogenic source emissions of aerosols on AOD due to the clean air acts. The relative importance of the two processes leading to reduction of CA over ASMR remains to be determined in further studies.

Finally, we note that even with the assimilation of winds and AOD in MERRA-2, the diagnostics we used based on vertical motions, precipitation, cloudiness, latent and radiative heating and tropopause height to define the climate states of the ASM and feedback effects on UTLS transport processes are likely dependent on model and data assimilation system (Fujiwara & Coauthors et al., 2017; SPARC, 2022). In this regard, the results of this study should be considered as highly exploratory, and should be taken with extreme caution. Future work based on intercomparison of multiple re-analyses and available observations of UTLS pollutants for trajectory analyses of wildfires events in northern Eurasia boreal forest regions are needed to reduce uncertainties and advance deeper understanding.

Data Availability Statement

All data used for this research are available online. MERRA-2, QFED, IMERG rainfall are available from the NASA Goddard Earth Sciences (GES) Data and Information Services Center (DISC; <https://disc.sci.gsfc.nasa.gov/>); GPCP precipitation from (<http://gpcp.umd.edu/>). MODIS fire pixel count and Fire Radiative Power from (<https://feer.gsfc.nasa.gov/>), and EDGAR surface emission from (https://edgar.jrc.ec.europa.eu/dataset_ap50).

Acknowledgments

This work was supported by NASA Modeling and Analysis Program, Grant CA# 80NSSC17K0213 to the University of Maryland, and to the NASA Goddard Space Flight Center. Partial support to the senior author was also provided by the U.S. Department of Energy (DOE), Office of Science, Biological and Environmental Research as part of the Regional and Global Modeling and Analysis Program under Grant Award #300426-00001 to University of Maryland from the Pacific Northwest National Laboratory (PNNL). PNNL is operated for DOE, by Battelle Memorial Institute under contract DE-AC05-76RL01830.

References

- Abalos, M., Randel, W. J., & Serrano, E. (2012). Variability in upwelling across the tropical tropopause and correlations with tracers in the lower stratosphere. *Atmospheric Chemistry and Physics*, 12(23), 11505–11517. <https://doi.org/10.5194/acp-12-11505-2012>
- Bacmeister, J. T., Suarez, M. J., & Robertson, F. R. (2006). Rain re-evaporation, boundary layer-convection interactions, and Pacific rainfall patterns in an AGCM. *Journal of the Atmospheric Sciences*, 63(12), 3383–3403. <https://doi.org/10.1175/jas3791.1>
- Basha, G., Ratnam, M. V., & Kishore, P. (2020). Asian summer monsoon anticyclone: Trends and variability. *Atmospheric Chemistry and Physics*, 20(11), 6789–6801. <https://doi.org/10.5194/acp-20-6789-2020>
- Bian, J., Li, D., Bai, Z., Li, Q., Lyu, D., & Zhou, X. (2020). Transport of Asian surface pollutants to the global stratosphere from the Tibetan Plateau region during the Asian summer monsoon. *National Science Review*, 7(3), 516–533. <https://doi.org/10.1093/nsr/nwaa005>
- Boothe, A. C., & Homeyer, C. R. (2017). Global large-scale stratosphere-troposphere exchange in modern reanalyses. *Atmospheric Chemistry and Physics*, 17(9), 5537–5559. <https://doi.org/10.5194/acp-17-5537-2017>
- Bossolasco, A., Jegou, F., Sellitto, P., Berthet, G., Kloss, C., & Legras, B. (2021). Global modeling studies of composition and decadal trends of the Asian Tropopause Aerosol Layer. *Atmospheric Chemistry and Physics*, 21(4), 2745–2764. <https://doi.org/10.5194/acp-21-2745-2021>
- Buchard, V., Randles, C. A., da Silva, A. M., Darmenov, A., Colarco, P. R., Govindaraju, R., et al. (2017). The MERRA-2 aerosol reanalysis, 1980 onward. Part II: Evaluation and case studies. *Journal of Climate*, 30(17), 6851–6872. <https://doi.org/10.1175/jcli-d-16-0613.1>

- Byrne, M. P., & Schneider, T. (2016). Narrowing of the ITCZ in a warming climate: Physical mechanisms. *Geophysical Research Letters*, 43(21), 11350–11357. <https://doi.org/10.1002/2016GL070396>
- Christian, K., Wang, J., Ge, C., Peterson, D., Hyer, E., Yorks, J., & McGill, M. (2019). Radiative forcing and stratospheric warming of pyro-cumulonimbus smoke aerosols: First modeling results with multi-sensor (EPIC, CALIPSO, and CATS) views from space. *Geophysical Research Letters*, 46(16), 10061–10071. <https://doi.org/10.1029/2019GL082360>
- Clemens, J., Ploeger, F., Konopka, P., Portmann, R., Sprenger, M., & Wernli, H. (2022). Characterization of transport from the Asian summer monsoon anticyclone into the UTLS via shedding of low potential vorticity cutoffs. *Atmospheric Chemistry and Physics*, 22(6), 3841–3860. <https://doi.org/10.5194/acp-22-3841-2022>
- Cunningham, P., & Reeder, M. J. (2009). Severe convective storms initiated by intense wildfires: Numerical simulations of pyro-convection and pyro-tornadogenesis. *Geophysical Research Letters*, 36(12), L12812. <https://doi.org/10.1029/2009GL039262>
- D'Agostino, R., Scambiat, A. L., Jungclaus, J., & Lionello, P. (2020). Poleward shift of northern subtropics in winter: Time of emergence of zonal versus regional signals. *Geophysical Research Letters*, 47, e2020GL089325. <https://doi.org/10.1029/2020GL089325>
- Dai, A. (2013). Increasing drought under global warming in observations and models. *Nature Climate Change*, 3(1), 52–58. <https://doi.org/10.1038/nclimate1633>
- d'Almeida, G. A., Koepke, P., & Shettle, E. P. (1991). In A. Deepak, (Ed.), *Atmospheric aerosols-global climatology and radiative characteristics*. Darnenov, A., & da Silva, A. (2015). The Quick Fire Emissions Data Set (QFED): Documentation of versions 2.1, 2.2, and 2.4 NASA/Tech. Memo-2015-104606.
- Diehl, T., Heil, A., Chin, M., Pan, X., Streets, D., Schultz, M., & Kinne, S. (2012). Anthropogenic, biomass burning, and volcanic emissions of black carbon, organic carbon, and SO₂ from 1980 to 2010 for hindcast model experiments. *Atmospheric Chemistry and Physics*, 12, 24895–24954. <https://doi.org/10.5194/acpd-12-24895-2012>
- Duncan, B. N., Martin, R. V., Staudt, A. C., Yevich, R., & Logan, J. A. (2003). Interannual and seasonal variability of biomass burning emissions constrained by satellite observations. *Journal of Geophysical Research*, 108(D2), 4040. <https://doi.org/10.1029/2002JD002378>
- Dunkerton, T. J. (1995). Evidence of meridional motion in the summer lower stratosphere adjacent to monsoon regions. *Journal of Geophysical Research*, 100(D8), 16675–16688. <https://doi.org/10.1029/95jd01263>
- Dvortsov, V. L., & Solomon, S. (2001). Response of the stratospheric temperatures and ozone to past and future increases in stratospheric humidity. *Journal of Geophysical Research*, 106(D7), 7505–7514. <https://doi.org/10.1029/2000JD900637>
- Enomoto, T., Hoskins, B. J., & Matsuda, Y. (2003). The formation mechanism of the Bonin high in August. *Quarterly Journal of the Royal Meteorological Society*, 129(587), 157–178. <https://doi.org/10.1256/qj.01.211>
- European Commission. (2011). European Commission/Joint Research Centre (JRC)/Netherlands Environmental Assessment Agency (PBL). Emission Database for Global Atmospheric Research (EDGAR), release version 4.2. Retrieved from <http://edgar.jrc.ec.europa.eu>
- Fadnavis, S., Kalita, G., Kumar, K. R., Gasparini, B., & Li, J.-L. F. (2017). Potential impact of carbonaceous aerosol on the upper troposphere and lower stratosphere (UTLS) and precipitation during Asian summer monsoon in a global model simulation. *Atmospheric Chemistry and Physics*, 17(18), 11637–11654. <https://doi.org/10.5194/acp-17-11637-2017>
- Fadnavis, S., Sabin, T. P., Roy, C., Rowlinson, M., Rap, A., Vernier, J.-P., & Sioris, C. E. (2019). Elevated aerosol layer over South Asia worsens the Indian droughts. *Scientific Reports*, 9(1), 10268. <https://doi.org/10.1038/s41598-019-46704-9>
- Fadnavis, S., Semeniuk, K., Pozzoli, L., Schultz, M. G., Ghude, S. D., Das, S., & Kakatkar, R. (2013). Transport of aerosols into the UTLS and their impact on the Asian monsoon region as seen in a global model simulation. *Atmospheric Chemistry and Physics*, 13(17), 8771–8786. <https://doi.org/10.5194/acp-13-8771-2013>
- Fan, J., Wang, Y., Rosenfeld, D., & Liu, X. (2016). Review of aerosol-cloud interactions: Mechanisms, significance, and challenges. *Journal of the Atmospheric Sciences*, 73(11), 4221–4252. <https://doi.org/10.1175/jas-d-16-0037.1>
- Fan, Q., Bian, J., & Pan, L. L. (2017). Stratospheric entry point for upper-tropospheric air within the Asian summer monsoon anticyclone. *Science China Earth Sciences*, 60(9), 1685–1693. <https://doi.org/10.1007/s11430-016-9073-5>
- Forster, P. M., & Shine, K. P. (1999). Stratospheric water vapor changes as a possible contributor to observed stratospheric cooling. *Geophysical Research Letters*, 26(21), 3309–3312. <https://doi.org/10.1029/1999gl010487>
- Forster, P. M., & Shine, K. P. (2002). Assessing the climate impact of trends in stratospheric water vapor. *Geophysical Research Letters*, 29(6), 10–11. <https://doi.org/10.1029/2001GL013909>
- Frey, W., Schofield, R., Hoor, P., Kunkel, D., Ravegnani, F., Ulanovsky, A., et al. (2015). The impact of overshooting deep convection on local transport and mixing in the tropical upper troposphere/lower stratosphere (UTLS). *Atmospheric Chemistry and Physics*, 15(11), 6467–6486. <https://doi.org/10.5194/acp-15-6467-2015>
- Fueglistaler, S., Dessler, A. E., Dunkerton, T. J., Folkins, I., Fu, Q., & Mote, P. W. (2009). Tropical tropopause layer. *Reviews of Geophysics*, 47(1), RG1004. <https://doi.org/10.1029/2008RG000267>
- Fujiwara, M., Wright, J. S., Manney, G. L., Gray, L. J., Anstey, J., Birner, T., et al. (2017). Introduction to the SPARC Reanalysis Intercomparison Project (S-RIP) and overview of the reanalysis systems. *Atmospheric Chemistry and Physics*, 17(2), 1417–1452. <https://doi.org/10.5194/acp-17-1417-2017>
- Gayatri, K., Kunchala, R. K., Fadnavis, S., & Kaskaoutis, D. G. (2020). Long-term variability of carbonaceous aerosols over Southeast Asia via reanalysis: Association with changes in vegetation cover and biomass burning. *Atmospheric Research*, 245, 05064. ISSN 0169-8095. <https://doi.org/10.1016/j.atmosres.2020.105064>
- Ge, J., You, Q., & Zhang, Y. (2018). The influence of the Asian summer monsoon onset on the northward movement of the South Asian high towards the Tibetan Plateau and its thermodynamic mechanism. *International Journal of Climatology*, 38(2), 543–553. <https://doi.org/10.1002/joc.5192>
- Gelaro, R., McCarty, W., Suarez, M. J., Todling, R., Molod, A., Takacs, L., et al. (2017). The Modern-Era Retrospective Analyses for Research and Applications, Version 2 (MERRA-2). *Journal of Climate*, 30(14), 5419–5454. <https://doi.org/10.1175/jcli-d-16-0758.1>
- Gottelman, A., Birner, T., Eyring, V., Akiyoshi, H., Bekki, S., Bruhl, C., et al. (2009). The tropical tropopause layer 1960–2100. *Atmospheric Chemistry and Physics*, 9(5), 1621–1637. <https://doi.org/10.5194/acp-9-1621-2009>
- Gottelman, A., Hegglin, M. I., Son, S. W., Kim, J., Fujiwara, M., Birner, T., et al. (2010). Multi-model assessment of the upper troposphere and lower stratosphere: Tropics and global trends. *Journal of Geophysical Research*, 115, D00M08. <https://doi.org/10.1029/2009JD013638>
- Gottelman, A., Salby, M. L., & Sassi, F. (2002). The distribution and influence of convection in the tropical tropopause region. *Journal of Geophysical Research*, 107(D10), ACL6-1–ACL6-12. <https://doi.org/10.1029/2001JD001048>
- Gill, A. E. (1980). Some simple solutions for heat-induced tropical circulation. *Quarterly Journal of the Royal Meteorological Society*, 106(449), 447–462. <https://doi.org/10.1002/qj.49710644905>

- Groisman, P. Y., Sherstyukov, B. G., Razuvaev, V. N., Knight, R. W., Enloe, J. G., Stroumentova, N. S., et al. (2007). Potential forest fire danger over Northern Eurasia: Changes during the 20th century. *Global and Planetary Change*, 56(3–4), 371–386. ISSN 0921-8181. <https://doi.org/10.1016/j.gloplacha.2006.07.029>
- Han, Y., Ma, W., Yao, Y., Yang, M., Xie, Z., Sun, G., et al. (2021). Impacts of the Silk Road pattern on the interdecadal variations of the atmospheric heat source over the Tibetan Plateau. *Atmospheric Research*, 260, 05696. ISSN 0169-8095. <https://doi.org/10.1016/j.atmosres.2021.105696>
- Hartmann, D. L., Wallace, J. M., Limpasuvan, V., Thompson, D., & Holton, J. R. (2000). Can ozone depletion and global warming interact to produce rapid climate change? *Proceedings of the National Academy of Sciences*, 97(4), 1412–1417. <https://doi.org/10.1073/pnas.97.4.1412>
- Hendricks, J., Kärcher, B., & Lohmann, U. (2011). Effects of ice nuclei on cirrus clouds in a global climate model. *Journal of Geophysical Research*, 116(D18), D18206. <https://doi.org/10.1029/2010JD015302>
- Holton, J. R., Haynes, P. H., McIntyre, M. E., Douglass, A. R., Rood, R. B., & Pfister, L. (1995). Stratosphere-troposphere exchange. *Reviews of Geophysics*, 33(4), 403–439. <https://doi.org/10.1029/95RG02097>
- Homeyer, C. R., & Bowman, K. P. (2013). Rossby wave breaking and transport between the tropics and extratropics above the subtropical jet. *Journal of the Atmospheric Sciences*, 70(2), 607–626. <https://doi.org/10.1175/jas-d-12-0198.1>
- Hong, X., & Lu, R. (2016). The meridional displacement of the summer Asia Jet, Silk Road Pattern, and tropical SST anomalies. *Journal of Climate*, 29(10), 3753–3766. <https://doi.org/10.1175/JCLI-D-15-0541.1>
- Honovich, S. B., & Pan, L. L. (2020). Transport from the Asian summer monsoon anticyclone over the western Pacific. *Journal of Geophysical Research*, 125(13), e2019JD032094. <https://doi.org/10.1029/2019JD032094>
- Hsu, H.-H., Terng, C. T., & Chen, C.-T. (1999). Evolution of large-scale circulation and heating during the first transition of Asian summer monsoon. *Journal of Climate*, 12(3), 793–810. [https://doi.org/10.1175/1520-0442\(1999\)012<0793:eolsca>2.0.co;2](https://doi.org/10.1175/1520-0442(1999)012<0793:eolsca>2.0.co;2)
- Janssens-Maenhout, G., Crippa, M., Guizzardi, D., Muntean, M., Schaaf, E., Dentener, F., et al. (2019). EDGAR v4.3.2 Global Atlas of the three major greenhouse gas emissions for the period 1970–2012. *Earth System Science Data*, 11(3), 959–1002. <https://doi.org/10.5194/essd-11-959-2019>
- Ji, Z., Kang, S., Cong, Z., Zhang, Q., & Yao, T. (2015). Simulation of carbonaceous aerosols over the Third Pole and adjacent regions: Distribution, transportation, deposition, and climatic effects. *Climate Dynamics*, 45(9–10), 2831–2846. <https://doi.org/10.1007/s00382-015-2509-1>
- Kharuk, V. I., Ponomarev, E. I., Ivanova, G. A., Dvinskaya, M. L., Coogan, S. C. P., & Flannigan, M. D. (2021). Wildfires in the Siberian taiga. *Ambio*, 50(11), 1953–1974. <https://doi.org/10.1007/s13280-020-01490-x>
- Kim, J., Randel, W. J., & Birner, T. (2018). Convectively driven tropopause-level cooling and its influences on stratospheric moisture. *Journal of Geophysical Research: Atmospheres*, 123(1), 590–606. <https://doi.org/10.1002/2017JD027080>
- Kim, M. K., Lau, W. K. M., Kim, K.-M., Sang, J., Kim, Y.-H., & Lee, W.-S. (2015). Amplification of ENSO effects on Indian summer monsoon by absorbing aerosols. *Climate Dynamics*, 46(7–8), 2657–2671. <https://doi.org/10.1007/s00382-015-2722-y>
- Krishnamurti, T. N., Daggupati, S. M., Fein, J., Kanamitsu, M., & Lee, J. D. (1973). Tibetan high and upper tropospheric tropical circulations during northern summer. *Bulletin of the American Meteorological Society*, 54(12), 1234–1250. <https://doi.org/10.1175/1520-0477.54.12.1234>
- Lau, K. M., Kim, M. K., & Kim, K. M. (2006). Aerosol induced anomalies in the Asian summer monsoon: The role of the Tibetan Plateau. *Climate Dynamics*, 26(7–8), 855–864. <https://doi.org/10.1007/s00382-006-0114-z>
- Lau, K. M., Ramanathan, V., Wu, G. X., Li, Z., Tsay, S. C., Hsu, C., et al. (2008). The joint aerosol-monsoon experiment: A new challenge in monsoon climate research. *Bulletin of the American Meteorological Society*, 89(3), 369–383. <https://doi.org/10.1175/bams-89-3-369>
- Lau, K. M., Wu, H. T., & Kim, K. M. (2013). A canonical response in rainfall characteristics to global warming from CMIP5 model projections. *Geophysical Research Letters*, 40(12), 3163–3169. <https://doi.org/10.1002/grl.50420>
- Lau, W. K. M. (2016). The aerosol-monsoon climate system of Asia: A new paradigm. *Journal of Meteorological Research*, 29(6), 1–11. <https://doi.org/10.1007/s13351-015-5999-1>
- Lau, W. K. M., & Kim, K. M. (2015). Robust responses of the Hadley circulation and global dryness in CMIP5 model CO₂ warming projections. *Proceedings of the National Academy of Sciences*, 112(12), 3630–3635. <https://doi.org/10.1073/pnas.1418682112>
- Lau, W. K. M., Kim, K. M., Shi, J. J., Matsui, T., Chin, M., Tan, Q., et al. (2016). Impacts of aerosol-monsoon interaction on rainfall and circulation over Northern India and the Himalaya Foothills. *Climate Dynamics*, 49(5), 1945–1960. <https://doi.org/10.1007/s00382-016-3430-y>
- Lau, W. K. M., Kim, K. M., Zhou, C., Leung, R. L., & Park, S. H. (2020). Impact of dust-cloud-radiation-precipitation dynamical feedback on S2S variability of the Asian summer monsoon in a global variable simulation with MPAS-CAM5. *Frontier in Atmospheric Science*. <https://doi.org/10.3389/feart.2020.00226>
- Lau, W. K. M., Yuan, M. C., & Li, Z. (2018). Origin, maintenance and variability of the Asian Tropopause Aerosol Layer (ATAL): Roles of monsoon dynamics. *Sci Reports*, 8(1), 3960. <https://doi.org/10.1038/s41598-018-22267-z>
- Li, Z., Lau, W. K.-M., Ramanathan, V., Wu, G., Ding, Y., Manoj, M. G., et al. (2016). Aerosol and monsoon climate interactions over Asia. *Reviews of Geophysics*, 54(4), 866–929. <https://doi.org/10.1002/2015rg000500>
- Liu, B., Wu, G., Mao, J., & He, J. (2013). Genesis of the South Asian high and its impact on the Asian summer monsoon onset. *Journal of Climate*, 26(9), 2976–2991. <https://doi.org/10.1175/jcli-d-12-00286.1>
- Liu, Y., Zhou, W., Qu, X., & Wu, R. (2020). An interdecadal change of the boreal summer Silk Road pattern around the late 1990s. *Journal of Climate*, 33(16), 7083–7100. <https://doi.org/10.1175/jcli-d-19-0795.1>
- Manney, G. L., & Hegglin, M. I. (2018). Seasonal and regional variations in long-term changes in upper tropospheric jets from reanalyses. *Journal of Climate*, 31(1), 423–448. <https://doi.org/10.1175/JCLI-D-17-0303.1>
- Manney, G. L., Hegglin, M. I., Daffer, W. H., Santee, M. L., Ray, E. A., Pawson, S., et al. (2011). Jet characterization in the upper troposphere/lower stratosphere (UTLS): Applications to climatology and transport studies. *Atmospheric Chemistry and Physics*, 11(12), 6115–6137. <https://doi.org/10.5194/acp-11-6115-2011>
- Manney, G. L., Santee, M. L., Lawrence, Z. D., Wargan, K., & Schwartz, M. J. (2021). A moments view of climatology and variability of the Asian summer monsoon anticyclone. *Journal of Climate*, 34(19), 7821–7841. <https://doi.org/10.1175/jcli-d-20-0729.1>
- Meng, Y., Deng, Y., & Shi, P. (2015). Mapping forest wildfire risk of the world. In P. Shi, & R. Kaspersen (Eds.), *World Atlas of Natural Disaster Risk, IHDP/Future Earth-Integrated Risk Governance Project Series*. Springer. https://doi.org/10.1007/978-3-662-45430-5_14
- Mokhov, I. I., & Chernokulsky, A. V. (2010). Regional model assessments of forest fire risks in the Asian part of Russia under climate change. *Geography and Natural Resources*, 31(2), 165–169. <https://doi.org/10.1016/j.gnr.2010.06.012>
- Molod, A. (2012). Constraints on the profiles of total water PDF in AGCMs from AIRS and a high-resolution model. *Journal of Climate*, 25(23), 8341–8352. <https://doi.org/10.1175/jcli-d-11-00412.1>
- Molod, A., Takacs, L., Suarez, M., & Bacmeister, J. (2015). Development of the GEOS-5 atmospheric general circulation model: Evolution from MERRA to MERRA2. *Geoscientific Model Development*, 8(5), 1339–1356. <https://doi.org/10.5194/gmd-8-1339-2015>

- Müller, S., Hoor, P., Bozem, H., Gute, E., Vogel, B., Zahn, A., et al. (2016). Impact of the Asian monsoon on the extratropical lower stratosphere: Trace gas observations during TACTS over Europe 2012. *Atmospheric Chemistry and Physics*, 16, 10573–10589. <https://doi.org/10.5194/acp-16-10573-2016>
- Munchak, L. A., & Pan, L. L. (2014). Separation of the lapse rate and the cold point tropopauses in the tropics and the resulting impact on cloud top-tropopause relationships. *Journal of Geophysical Research: Atmospheres*, 119(13), 7963–7978. <https://doi.org/10.1002/2013JD021189>
- Pan, L. L., Bowman, K. P., Atlas, E. L., Wofsy, S. C., Zhang, F., Bresch, J. F., et al. (2010). The stratosphere-troposphere analyses of regional transport 2008 experiment. *Bulletin of the American Meteorological Society*, 91(3), 327–342. <https://doi.org/10.1175/2009bams2865.1>
- Pan, L. L., Honomichl, S. B., Bui, T. V., Thornberry, T., Rollins, A., Hints, E., & Jensen, E. J. (2018). Lapse rate or cold point: The tropical tropopause identified by in situ trace gas measurements. *Geophysical Research Letters*, 45, 10756–10763. <https://doi.org/10.1029/2018GL079573>
- Pan, L. L., Honomichl, S. B., Kinnison, D. E., Abalos, M., Randel, W. J., Bergman, J. W., & Bian, J. (2016). Transport of chemical tracers from the boundary layer to stratosphere associated with the dynamics of the Asian summer monsoon. *Journal of Geophysical Research: Atmospheres*, 121(23), 14159–14174. <https://doi.org/10.1002/2016JD025616>
- Pan, L. L., Paulik, L. C., Honomichl, S. B., Munchak, L. A., Bian, J., Selkirk, H. B., & Vömel, H. (2014). Identification of the tropical tropopause transition layer using the ozone-water vapor relationship. *Journal of Geophysical Research: Atmospheres*, 119(6), 3586–3599. <https://doi.org/10.1002/2013JD020558>
- Park, M., Randel, W. J., Emmons, L. K., & Livesey, N. J. (2009). Transport pathways of carbon monoxide in the Asian summer monsoon diagnosed from Model of Ozone and Related Tracers (MOZART). *Journal of Geophysical Research*, 114(D8), D08303. <https://doi.org/10.1029/2008JD010621>
- Park, M., Randel, W. J., Gettelman, A., Massie, S. T., & Jiang, J. H. (2007). Transport above the Asian summer monsoon anticyclone inferred from Aura Microwave Limb Sounder tracers. *Journal of Geophysical Research*, 112(D16), D16309. <https://doi.org/10.1029/2006JD008294>
- Phoenix, D. B., Homeyer, C. R., Barth, M. C., & Trier, S. B. (2020). Mechanisms responsible for stratosphere-to-troposphere transport around a mesoscale convective system anvil. *Journal of Geophysical Research: Atmospheres*, 125(10), e2019JD032016. <https://doi.org/10.1029/2019JD032016>
- Ploeger, F., Fueglistaler, S., Grooß, J.-U., Günther, G., Konopka, P., Liu, Y. S., et al. (2011). Insight from ozone and water vapor on transport in the tropical tropopause layer (TTL). *Atmospheric Chemistry and Physics*, 11(1), 407–419. <https://doi.org/10.5194/acp-11-407-2011>
- Ploeger, F., Konopka, P., Müller, R., Fueglistaler, S., Schmidt, T., Manners, J. C., et al. (2012). Horizontal transport affecting trace gas seasonality in the Tropical Tropopause Layer (TTL). *Journal of Geophysical Research*, 117(D9), D09303. <https://doi.org/10.1029/2011JD017267>
- Preethi, B., Mujumdar, M., Kripalani, R. H., Prabhu, A., & Krishnan, R. (2017). Recent trends and tele-connections among South and East Asian summer monsoons in a warming environment. *Climate Dynamics*, 48(7–8), 2489–2505. <https://doi.org/10.1007/s00382-016-3218-0>
- Raga, G. B., Baumgardner, D., Rios, B., Díaz-Esteban, Y., Jaramillo, A., Gallagher, M., et al. (2022). High concentrations of ice crystals in upper-tropospheric tropical clouds: Is there a link to biomass and fossil fuel combustion? *Atmospheric Chemistry and Physics*, 22(4), 2269–2292. <https://doi.org/10.5194/acp-22-2269-2022>
- Randel, W. J., & Jensen, E. (2013). Physical processes in the tropical tropopause layer and their role in a changing climate. *Nature Geoscience*, 6(3), 169–176. <https://doi.org/10.1038/ngeo1733>
- Randel, W. J., & Park, M. (2006). Deep convective influence on the Asian summer monsoon anticyclone and associated tracer variability observed with Atmospheric Infrared Sounder (AIRS). *Journal of Geophysical Research*, 111(D12), D12314. <https://doi.org/10.1029/2005JD006490>
- Randel, W. J., Park, M., Emmons, L., Kinnison, D., Bernath, P., Walker, K. A., et al. (2010). Asian monsoon transport of pollution to the stratosphere. *Science*, 328(5978), 611–613. <https://doi.org/10.1126/science.1182274>
- Randerson, J. T., vander Werf, G. R., Giglio, L., Collatz, G. J., & Kasibhatla, P. S. (2017). *Global Fire Emissions Database, Version 4.1 (GFEDv4)*. ORNL DAAC. <https://doi.org/10.3334/ORNLDAAAC/1293>
- Randles, C. A., da Silva, A. M., Buchard, V., Colarco, P. R., Darmenov, A., Govindaraju, R., et al. (2017). The MERRA-2 aerosol reanalysis, 1980 onward. Part I: System description and data assimilation evaluation. *Journal of Climate*, 30(17), 6823–6850. <https://doi.org/10.1175/jcli-d-16-0609.1>
- Reichle, R. H., Liu, Q., Koster, R. D., Draper, C. S., Mahanama, S. P., & Partyka, G. S. (2017). Land surface precipitation in MERRA-2. *Journal of Climate*, 30(5), 1643–1664. <https://doi.org/10.1175/JCLI-D-16-0570.1>
- Riese, M., Ploeger, F., Rap, A., Vogel, B., Konopka, P., Dameris, M., & Forster, P. (2012). Impact of uncertainties in atmospheric mixing on simulated UTLS composition and related radiative effects. *Journal of Geophysical Research*, 117(D16), D16305. <https://doi.org/10.1029/2012JD017751>
- Rosenfeld, D., Andreae, M. O., Asmi, A., Chin, M., de Leeuw, G., Donovan, D. P., et al. (2014). Global observations of aerosol-cloud-precipitation-climate interactions. *Reviews of Geophysics*, 52(4), 750–808. <https://doi.org/10.1002/2013RG000441>
- Rosenfeld, D., Lohmann, U., Raga, G. B., O'Dowd, C. D., Kulmala, M., Fuzzi, S., et al. (2008). Flood or drought: How do aerosols affect precipitation? *Science*, 321(5894), 1309–1313. <https://doi.org/10.1126/science.1160606>
- Rosenfeld, D., & Woodley, W. (2000). Deep convective clouds with sustained supercooled liquid water down to -37.5°C . *Nature*, 405(6785), 440–442. <https://doi.org/10.1038/35013030>
- Rosenlof, K. H., & Reid, G. C. (2008). Trends in the temperature and water vapor content of the tropical lower stratosphere: Sea surface connection. *Journal of Geophysical Research*, 113(D6), D06107. <https://doi.org/10.1029/2007JD009109>
- Samanta, D., Dash, M. K., Goswami, B. N., & Pandey, P. C. (2016). Extratropical anticyclonic wave breaking and Indian summer monsoon failure. *Climate Dynamics*, 46(5–6), 1547–1562. <https://doi.org/10.1007/s00382-015-2661-7>
- Santee, M. L., Manney, G. L., Livesey, N. J., Schwartz, M. J., Neu, J. L., & Read, W. G. (2017). A comprehensive overview of the climatological composition of the Asian summer monsoon anticyclone based on 10 yr of Aura Microwave Limb Sounder measurements. *Journal of Geophysical Research*, 122, 5491–5514. <https://doi.org/10.1002/2016JD026408>
- Santer, B. D., Sausen, R., Wigley, T. M. L., Boyle, J. S., AchutaRao, K., Doutriaux, C., et al. (2003). Behavior of tropopause height and atmospheric temperature in models, reanalyses, and observations: Decadal changes. *Journal of Geophysical Research*, 108(D1), 4002. <https://doi.org/10.1029/2002JD002258>
- Santer, B. D., Wehner, M. F., Wigley, T. M. L., Sausen, R., Meehl, G. A., Taylor, K. E., et al. (2003). Contribution of anthropogenic and natural forcing to recent tropopause height change. *Science*, 25(5632), 479–483. <https://doi.org/10.1126/science.1084123>
- Satheesh, S. K., & Moorthy, K. (2005). Radiative effect of natural aerosols: A review. *Atmospheric Environment*, 39, 2089–2110. <https://doi.org/10.1016/j.atmosenv.2004.12.029>
- Seidel, D. J., Fu, Q., Randel, W., & Reichler, T. J. (2008). Widening of the tropical belt in a changing climate. *Nature Geoscience*, 1, 21–24. <https://doi.org/10.1038/ngeo.2007.38>
- Seidel, D. J., & Randel, W. J. (2006). Variability and trends in the global tropopause estimated from radiosonde data. *Journal of Geophysical Research*, 111(D21), D21101. <https://doi.org/10.1029/2006JD007363>

- Shepherd, T. G. (2008). Dynamics, stratospheric ozone, and climate change. *Atmosphere-Ocean*, 46(1), 117–138. <https://doi.org/10.3137/ao.460106>
- Shi, C., Huang, Y., Guo, D., Zhou, S., Hu, K., & Liu, Y. (2018). Comparison of trends and abrupt changes of the South Asia high from 1979 to 2014 in reanalysis and radiosonde datasets. *Journal of Atmospheric and Solar-Terrestrial Physics*, 170, 48–54. <https://doi.org/10.1016/j.jastp.2018.02.005>
- Shi, N., Wang, Y., Wang, X., & Tian, P. (2019). Interdecadal variations in the frequency of persistent hot events in boreal summer over midlatitude Eurasia. *Journal of Climate*, 32(16), 5161–5177. <https://doi.org/10.1175/jcli-d-18-0706.1>
- Sohn, B. J., Yeh, S. W., Lee, A., & Lau, W. K. M. (2019). Regulation of atmospheric circulation controlling the tropical Pacific precipitation change in response to CO₂ increases. *Nature Communications*, 10(1), 1108. <https://doi.org/10.1038/s41467-019-08913-8>
- Solomon, S., Daniel, J. S., Neely, R. R., III, Vernier, J. P., Dutton, E. G., & Thomason, L. W. (2011). The persistently variable background stratospheric aerosol layer and global climate change. *Science*, 333(6044), 866–870. <https://doi.org/10.1126/science.1206027>
- Soto-García, L. L., Andreae, M. O., Andreae, T. W., Artaxo, P., Maenhaut, W., Kirchstetter, T., et al. (2011). Evaluation of the carbon content of aerosols from the burning of biomass in the Brazilian Amazon using thermal, optical, and thermal-optical analysis methods. *Atmospheric Chemistry and Physics*, 11(9), 4425–4444. <https://doi.org/10.5194/acp-11-4425-2011>
- SPARC. (2022). SPARC Reanalysis Intercomparison Project (S-RIP) Final Report. In G. L. Manney, L. J. Gray, & J. S. Wright (Eds.), *SPARC Report No. 10, WCRP-6/2021*. Retrieved from www.sparc-climate.org/publications/sparc-reports
- Staten, P. W., Grise, K. M., Davis, S. M., Karnauskas, K., & Davis, N. (2019). Regional widening of tropical overturning: Forced change, natural variability, and recent trends. *Journal of Geophysical Research: Atmospheres*, 124(12), 6104–6119. <https://doi.org/10.1029/2018JD030100>
- Stephan, C. C., Klingaman, N. P., & Turner, A. G. (2019). A mechanism for the recently increased interdecadal variability of the Silk Road pattern. *Journal of Climate*, 32(3), 717–736. <https://doi.org/10.1175/jcli-d-18-0405.1>
- Su, H., Jiang, J., Neelin, J., Shen, T. J., Zhai, C., Yue, Q., et al. (2017). Tightening of tropical ascent and high clouds key to precipitation change in a warmer climate. *Nature Communications*, 8(1), 15771. <https://doi.org/10.1038/ncomms15771>
- Takemura, K., & Mukougawa, H. (2020). Maintenance mechanism of Rossby wave breaking and Pacific-Japan pattern in boreal summer. *Journal of the Meteorological Society of Japan*, 98(6), 1183–1206. <https://doi.org/10.2151/jmsj.2020-061>
- Takemura, K., Mukougawa, H., & Maeda, S. (2020). Large-scale atmospheric circulation related to frequent Rossby wave breaking near Japan in boreal summer. *Journal of Climate*, 33(15), 6731–6744. <https://doi.org/10.1175/jcli-d-19-0958.1>
- Tegtmeier, S., Anstey, J., Davis, S., Dragani, R., Harada, Y., Ivanciu, I., et al. (2020). Temperature and tropopause characteristics from reanalyses data in the tropical tropopause layer. *Atmospheric Chemistry and Physics*, 20(2), 753–770. <https://doi.org/10.5194/acp-20-753-2020>
- Thomason, L. W., & Vernier, J.-P. (2013). Improved SAGE II cloud/aerosol categorization and observations of the Asian tropopause aerosol layer: 1989–2005. *Atmospheric Chemistry and Physics*, 13(9), 4605–4616. <https://doi.org/10.5194/acp-13-4605-2013>
- Trenberth, K., Dai, A., vander Schrier, G., Jones, P. D., Barichivich, J., Briffa, K. R., & Sheffield, J. (2014). Global warming and changes in drought. *Nature Climate Change*, 4(1), 17–22. <https://doi.org/10.1038/nclimate2067>
- Trentmann, J., Luderer, G., Winterrath, T., Fromm, M. D., Servranckx, R., Textor, C., et al. (2006). Modeling of biomass smoke injection into the lower stratosphere by a large forest fire (Part I): Reference simulation. *Atmospheric Chemistry and Physics*, 6(12), 5247–5260. <https://doi.org/10.5194/acp-6-5247-2006>
- van der Werf, G. R., Randerson, J. T., Giglio, L., van Leeuwen, T. T., Chen, Y., Rogers, B. M., et al. (2017). Global fire emissions estimates during 1997–2016. *Earth System Science Data*, 9(2), 697–720. <https://doi.org/10.5194/essd-9-697-2017>
- Vernier, J.-P., Fairlie, T. D., Natarajan, M., Wienhold, F. G., Bian, J., Martinsson, B. G., et al. (2015). Increase in upper tropospheric and lower stratospheric aerosol levels and its potential connection with Asian pollution. *Journal of Geophysical Research: Atmospheres*, 120(4), 1608–1619. <https://doi.org/10.1002/2014JD022372>
- Vernier, J.-P., Thomason, L. W., & Kar, J. (2011). CALIPSO detection of an Asian tropopause aerosol layer. *Geophysical Research Letters*, 38(7), L07804. <https://doi.org/10.1029/2010GL046614>
- Vogel, B., Günther, G., Müller, R., Groß, J.-U., Afchine, A., Bozem, H., et al. (2016). Long-range transport pathways of tropospheric source gases originating in Asia into the northern lower stratosphere during the Asian monsoon season 2012. *Atmospheric Chemistry and Physics*, 16(23), 15301–15325. <https://doi.org/10.5194/acp-16-15301-2016>
- Voigt, A., & Shaw, T. (2015). Circulation response to warming shaped by radiative changes of clouds and water vapor. *Nature Geoscience*, 8(2), 102–106. <https://doi.org/10.1038/ngeo2345>
- Wang, L., Xu, P., Chen, W., & Liu, Y. (2017). Interdecadal variations of the Silk Road pattern. *Journal of Climate*, 30(24), 9915–9932. <https://doi.org/10.1175/jcli-d-17-0340.1>
- Wang, S. X., Zhao, B., Cai, S. Y., Klimont, Z., Nielsen, C. P., Morikawa, T., et al. (2014). Emission trends and mitigation options for air pollutants in East Asia. *Atmospheric Chemistry and Physics*, 14(13), 6571–6603. <https://doi.org/10.5194/acp-14-6571-2014>
- Wilcox, L. J., Hoskins, B. J., & Shine, K. P. (2012). A global blended tropopause based on ERA data. Part II: Trends and tropical broadening. *Quarterly Journal of the Royal Meteorological Society*, 138(664), 576–584. <https://doi.org/10.1002/qj.910>
- Yan, F., He, C., Kang, S., Chen, P., Hu, Z., Han, X., et al. (2019). Deposition of organic and black carbon: Direct measurements at three remote stations in the Himalayas and Tibetan Plateau. *Journal of Geophysical Research: Atmospheres*, 124(16), 9702–9715. <https://doi.org/10.1029/2019JD031018>
- Yang, H., Chen, G., Tang, Q., & Hess, P. (2016). Quantifying isentropic stratosphere-troposphere exchange of ozone. *Journal of Geophysical Research: Atmospheres*, 121(7), 3372–3387. <https://doi.org/10.1002/2015JD024180>
- Yasunari, T. J., Kim, K. M., da Silva, A. M., Hayasaki, M., Akiyama, M., & Murao, N. (2018). Extreme air pollution events in Hokkaido, Japan, traced back to early snowmelt and large-scale wildfires over East Eurasia: Case studies. *Scientific Reports*, 8(1), 6413. <https://doi.org/10.1038/s41598-018-24335-w>
- Yasunari, T. J., Nakamura, H., Kim, K. M., Choi, N., Lee, M. I., Tachibana, T., & da Silva, A. M. (2021). Relationship between circum-Arctic atmospheric wave patterns and large-scale wildfires in boreal summer. *Environmental Research Letters*, 16(6), 064009. <https://doi.org/10.1088/1748-9326/abf7ef>
- Yu, P., Karen Rosenlof, K. H., Liu, S., Telg, H., Thornberry, T. D., Rollins, A. W., et al. (2017). Efficient transport of tropospheric aerosol into the stratosphere via the Asian summer monsoon anticyclone. *Proceedings of the National Academy of Sciences*, 114(27), 6972–6977. doi <https://doi.org/10.1073/pnas.1701170114>
- Yuan, C., Lau, W. K. M., Li, Z., & Cribb, M. (2019). Relationship between Asian monsoon strength and transport of surface aerosols to the Asian tropopause Aerosol Layer (ATAL): Interannual variability and decadal changes. *Atmospheric Chemistry and Physics*, 19(3), 1901–1913. <https://doi.org/10.5194/acp-19-1901-2019>
- Yun, K.-S., Timmermann, A., & Stuecker, M. F. (2021). Synchronized spatial shifts of Hadley and Walker circulations. *Earth System Dynamics*, 12(1), 121–132. <https://doi.org/10.5194/esd-12-121-2021>

- Zeng, Y., Cao, Y., Qiao, X., Seyler, B. C., & Tang, Y. (2019). Air pollution reduction in China: Recent success but great challenge for the future. *Science of the Total Environment*, 663, 329–337. SSN 0048-9697. <https://doi.org/10.1016/j.scitotenv.2019.01.262>
- Zhang, J., Chen, H., & Zhang, Q. (2019). Extreme drought in the recent two decades in northern China resulting from Eurasian warming. *Climate Dynamics*, 52(5–6), 2885–2902. <https://doi.org/10.1007/s00382-018-4312-2>
- Zheng, B., Chevallier, F., Ciais, P., Yin, Y., Deeter, M. N., Worden, H. M., et al. (2018). Rapid decline in carbon monoxide emissions and export from East Asia between years 2005–2016. *Environmental Research Letters*, 13(4), 044007. <https://doi.org/10.1088/1748-9326/aab2b3>
- Zhou, X.-L., Geller, M. A., & Zhang, M. (2001). Cooling trend of the tropical cold point tropopause temperatures and its implications. *Journal of Geophysical Research*, 106(D2), 1511–1522. <https://doi.org/10.1029/2000JD900472>